In silico trials predict that combination strategies for enhancing vesicular stomatitis oncolytic virus are determined by tumor aggressivity

Adrianne L Jenner [ORCID],[1,2] Tyler Cassidy [ORCID],[3,4] Katia Belaid,[2,5] Marie-Claude Bourgeois-Daigneault,[6,7] Morgan Craig [ORCID] [1,2]

Correspondence to
Dr Morgan Craig;
morgan.craig@umontreal.ca

ABSTRACT

Background Immunotherapies, driven by immune-mediated antitumorigenicity, offer the potential for significant improvements to the treatment of multiple cancer types. Identifying therapeutic strategies that bolster antitumor immunity while limiting immune suppression is critical to selecting treatment combinations and schedules that offer durable therapeutic benefits. Combination oncolytic virus (OV) therapy, wherein complementary OVs are administered in succession, offer such promise, yet their translation from preclinical studies to clinical implementation is a major challenge. Overcoming this obstacle requires answering fundamental questions about how to effectively design and tailor schedules to provide the most benefit to patients.

Methods We developed a computational biology model of combined oncolytic vaccinia (an enhancer virus) and vesicular stomatitis virus (VSV) calibrated to and validated against multiple data sources. We then optimized protocols in a cohort of heterogeneous virtual individuals by leveraging this model and our previously established in silico clinical trial platform.

Results Enhancer multiplicity was shown to have little to no impact on the average response to therapy. However, the duration of the VSV injection lag was found to be determinant for survival outcomes. Importantly, through treatment individualization, we found that optimal combination schedules are closely linked to tumor aggressivity. We predicted that patients with aggressively growing tumors required a single enhancer followed by a VSV injection 1 day later, whereas a small subset of patients with the slowest growing tumors needed multiple enhancers followed by a longer VSV delay of 15 days, suggesting that intrinsic tumor growth rates could inform the segregation of patients into clinical trials and ultimately determine patient survival. These results were validated in entirely new cohorts of virtual individuals with aggressive or non-aggressive subtypes.

Conclusions Based on our results, improved therapeutic schedules for combinations with enhancer OVs can be studied and implemented. Our results further underline the impact of interdisciplinary approaches to preclinical planning and the importance of computational approaches to drug discovery and development.

BACKGROUND

Oncolytic viruses (OVs) are genetically modified viruses designed to specifically target tumor cells.[1] The antitumor effects associated with oncolytic virotherapy are mediated significantly by immune mechanisms, which can be either advantageous or disadvantageous depending on the type of virus.[1] Although immunosuppression may improve viral oncolysis, this gain is achieved at the cost of antitumor immunity, a key factor for improving cancer therapies. The importance of considering immune-virus interactions is supported by the mechanism of action of the OV talimogene laherparepvec (T-VEC).[2] T-VEC was the first US Food and Drug Administration (FDA)-approved OV and is a genetically modified form of herpes simplex virus that encodes the immunostimulatory cytokine granulocyte-monocyte colony-stimulating factor (GM-CSF). The OV's effectiveness is amplified by its immunostimulatory counterpart,[3] attesting to the need to find a reasonable balance between a multitude of immune mechanisms (such as viral clearance and the antitumor immune response) to achieve ultimate treatment success.

Therapeutic cancer vaccines are administered to cancer patients with the goal of eradicating tumor cells through strengthening the patient's own immune response.[4] Combination OV protocols or vaccination schedules use a sequential combination of immunologically distinct viruses to induce immunity, circumvent or mitigate the antiviral immune response, and ultimately enhance antitumor efficacy.[5–7] Currently, there are three clinical trials investigating the efficacy of combining adenovirus and the OV Maraba as an anticancer vaccination treatment,[8 9] two of which are in the USA (NCT02285816; NCT02879760) and one in

Canada (control number 195876, protocol number: AD/ MG1-MAGEA3-001).

The principal idea behind combination OV regimens is to stimulate alternate mechanisms of antitumor immunity that act cooperatively or synergistically to enhance therapeutic effect. In this way, OVs can be used in enhancer virus/primary virus regimens whereby the pre-existing immune response induced by the enhancer OV will improve the efficacy of the second primary heterologous OV administration.[10] It has been shown that the development of an acquired antiviral immune response usually takes less than a week in treatment-naïve animals, leaving a small window of opportunity for oncolytic vectors to function.[11] Accepting that the ensuing immune response dictates that viral oncolysis will inevitably be transient in nature, the anti-OV immune response can be usefully reoriented to enhance the therapeutic impact of the vector.

Bridle *et al*[7] were among the first to investigate the synergy between combination OV therapies. They showed that the antitumor response to vesicular stomatitis virus (VSV) was weaker than the anti-VSV response. This led them to complement the initial injection of VSV with an injection of a different virus with the goal of harnessing the original anti-VSV response and improving the antitumor immune response. Bridle *et al*[12] therefore, investigated VSV as a boost to adenovirus antigen. They found that VSV antigen produced a more tumor-specific CD8+ T cell response which was more cytotoxic in combination with adenovirus-antigen with increased cytokine and granzyme production.

The exact immune mechanisms through which OVs induce antitumor responses depend on the type of virus used and the transgenes encoded. Ilett *et al*[1] showed that reovirus induced the priming of a CD8+, Th1-type antitumor response whereas VSV expression promoted a potent antitumor CD4 +Th17 response, and that priming with reovirus, followed by VSV significantly improved survival of B16 melanoma tumor-bearing mice versus virus alone. Previous work has also suggested that three low doses of adenovirus, followed by three low doses of vaccinia virus (VV) resulted in a superior antitumor efficacy versus six doses of either virus.[13]

Individually, VV and VSV have both been extensively investigated as possible oncolytic virotherapy agents.[11 13–18] Morphologically and immunologically, VSV and VV are very distinct. VV is a complex double stranded DNA virus encoding a large number of genes with immune evading properties that allow the virus to establish local pockets of infection within an infected host at a tissue level.[19] At the systemic level, VV is a highly immunogenic virus, eliciting strong T-cell-mediated and antibody responses.[20] Due to the role VV played in the worldwide smallpox eradication program, it has long been recognized as an efficient therapeutic vaccine and has the longest and most extensive history of human use of any virus, which demonstrates its safety.[20] In contrast, VSV is a genetically simple RNA virus (with only five gene products) that rapidly replicates and spreads within tumors. VSV is extremely sensitive to the antiviral effects of type I interferons (IFNs),[19] which act to inhibit viral replication and spread in immunocompetent (IC) hosts.[21 22]

The feasibility of using VV and VSV together in combination OV treatment was previously demonstrated, with the potential to improve therapeutic outcomes in triple negative breast cancer (TNBC).[19] Le Boeuf *et al*[19] used VV naturally expressing the viral gene product B18R, an IFN receptor decoy that locally antagonizes the cellular antiviral response initiated by type I IFNs, in parallel with a recombinant version of VSV expressing fusion-associated small-transmembrane protein to further enhance VV's ability to spread through an infected monolayer. The combination of these viruses resulted in a 'ping pong' oncolytic effect wherein VV enhanced the ability of VSV to replicate and/or spread in tumor cells. In their work, Le Boeuf *et al*[19] only considered a single administration of the combined dosage protocol (VV+VSV). A rational approach leveraging quantitative, predictive modeling and experimental results would help to delineate the therapeutic potential of combined enhancer VV with VSV, and further preclinical investigations into combined oncolytic virotherapy strategies.

The translation of OVs from preclinical studies to clinical implementation is a major challenge. Solving this obstacle requires answering fundamental questions about how to effectively design and tailor schedules to provide the most benefit to patients. Here, mathematical and computational biology help to identify strategies that offer durable therapeutic benefits prior to human trials.[23–32] Interpatient heterogeneity is a defining obstacle in cancer therapy, and patient-to-patient variability in cancer can cause finely tailored treatment protocols to exhibit extreme disparate antitumor responses.[33 34] Quantitative approaches have similarly been leveraged to integrate experimental data and identify robust optimal treatment protocols,[33] with quantitative systems pharmacology models contributing to decision making at the regulatory level.[35]

In particular, virtual clinical trials[36 37] (or in silico 'twins'[38 39]) have recently been used in preclinical research to make 'go or no go' decisions.[33 40–46] We have previously developed a computational biology model describing tumor-immune interactions and systemic cytokine concentrations over time,[47] which we used to determine the optimal combination of GM-CSF and OV.[46] We predicted that appropriately eliciting immune responses could significantly improve 5-year patient outcomes. Jafarnejad *et al*[48] conducted an in silico clinical trial of anti-PD-1 molecule nivolumab for non-small-cell lung cancer calibrated to human patient clinical trial data. They predicted that patients with adjuvant nivolumab treatment in addition to the clinical trial protocol of neoadjuvant nivolumab treatment, followed by resection produced a durable response. With a focus on cytotoxic T-lymphocyte-associated protein 4 (CTLA-4), programmed cell death protein 1 (PD-1) and

programmed death-ligand 1 (PD-L1) blockade in melanoma, Milberg et al[49] similarly leveraged a virtual clinical trial to predict the performance of therapeutic combinations given heterogeneous patient characteristics. Using their model validated to measurements from clinical trials, they predicted that response rates were higher for anti-PD-1/PD-L1 vs anti-CTLA-4/PD-1 combinations, and that anti-PD-1 administered before anti-CTLA-4 produced a greater response than the converse, consistent with clinical results. Applications of virtual patient 'twins' are not only specific to oncology but have also been applied in drug development, for example, to estimate the long-term effects of a treatment from short-term placebo-controlled trial measurements.[36 39]

Here, we expanded our mathematical model to investigate the therapeutic potential of enhancing VSV efficacy using VV as an enhancer. Using an in silico trial platform, we leveraged our computational biology model to predict tumor burden under clinically actionable combination OV-therapy administration schedules. Motivated by the results of Le Boeuf et al[19] where VV was shown to enhance the efficacy of VSV, we then interrogated the impact of enhancer (VV) multiplicity and the lag in VSV administration on tumor growth dynamics to establish an optimal enhancer number and VSV lag. Our results suggest that intrinsic tumor characteristics, mainly tumor aggressivity, are the primary drivers of therapeutic response and ultimate success. Importantly, we show that these attributes can be exploited for patient stratification and to tailor therapeutic protocols.

METHODS
Mathematical model of combination OV therapy and response
We extended our previous model for tumor growth and resistance to treatment with virotherapy and the resulting immune response[46] to consider the impact of using dual VV 'enhancer' and VSV OV injection. In this scenario, the antitumor immune response is either upregulated or downregulated depending on the type of virus injected. We considered total vaccinia and vesicular stomatitis virions ($V_{VV}(t)$ and $V_{VSV}(t)$, respectively) and two corresponding infected cell populations ($I_{VV}(t)$ and $I_{VSV}(t)$. Parameters from Cassidy and Craig[46] relating to viral kinetics were taken here to be virus dependent (subscript notation for κ, δ, α and ω). Additionally, we included an immunomodulation term $\rho \in [0,1]$ that modulates the production of immunostimulatory cytokines. The complete set of model equation is provided in the online supplemental technical information. A summary of the biological assumptions and model schematic is given in figure 1.

Briefly, the following biological interactions were added to the model described in Cassidy and Craig[46]:

▶ VSV and VV are morphologically and cytotoxically distinct[19] and therefore have the following virus-specific characteristics: virion-cell infection rates (κ_{VSV} and κ_{VV}), virion induced cell lysis rates (δ_{VSV} and δ_{VV}),
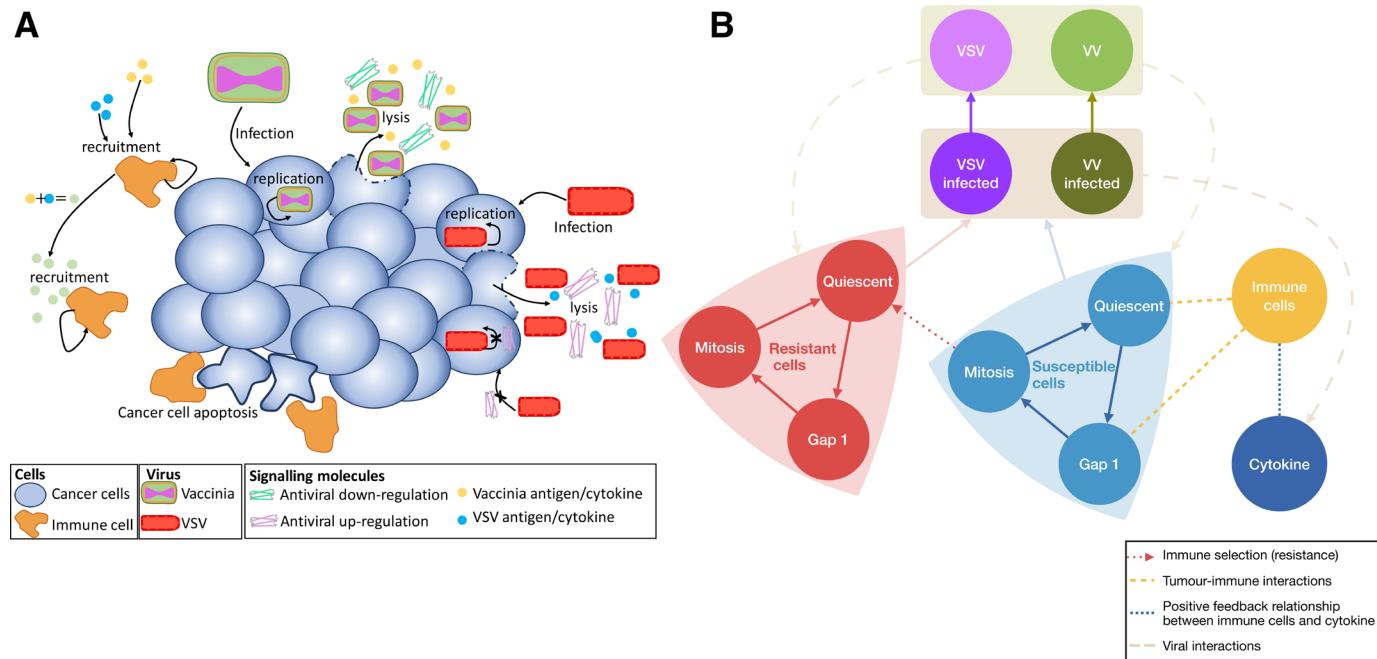
virion burst sizes (α_{VSV} and α_{VV}), and virion death rates (α_{VSV} and α_{VV}).

▶ Viruses modulate the production of cytokines through either promoting an inflammatory or anti-inflammatory immune response,[50] modeled through an immune modulation constant ($0 \leq \rho \leq 1$) that controls the rate of cytokine production from the immune interaction with cycling tumor cells (infected and uninfected). As $\rho \to 0$, cytokine production is reduced, recapitulating an anti-inflammatory immune regulation, and as $\rho \to 1$, normal inflammatory immune response is recovered.

▶ VV downregulates the production of antiviral factors, which aids the spread of VSV.[19] Therefore, we consider VV to downregulate cytokine production, instigating an anti-inflammatory response (ie, $\rho = 0$), whereas VSV upregulates cytokine production from both infected and uninfected tumor cells (ie, $\rho \approx 1$).

▶ Limitations on the binding of immune cells to cognate growth factors or signals[50] due to the simultaneous infection of both VV and VSV in the tumor were represented by higher production of inflammatory cytokines ($\rho = 1$) and a lower rate of maximal immune cell production (k_{cp}) when VSV particles are introduced after VV has commenced replication.

All other interactions are as in Cassidy and Craig.[46] For more information on the biological interactions and their model implementation see online supplemental technical information.

Estimation of vaccinia (VV) and VSV viral and immune related parameters
Parameters of the model were estimated via a hierarchical fitting algorithm in which subsets of the model were fit to different experiments using VV and VSV. Full details are provided in the online supplemental technical information. Briefly, we sequentially fit model parameters to the experimental measurements from HT29 and 4TI cell lines from Le Boeuf et al[19] and Rausch et al[51] (online supplemental figures TS1–TS3). Tumor growth parameters were obtained by fitting the rate quiescent cells enter the G_1 phase (a_1), the rate HT29 (human colorectal adenocarcinoma) and 4T1 (murine mammary carcinoma) cells leave G_1 to enter the active phase (a_2), and the rate cells undergo apoptosis in G_1 phase (d_2), in immunodeficient (ID) mice (ie, *HT29/ID* and *4T1/ID* obtained by Le Boeuf et al[19] and Rausch et al,[51] respectively). We then fixed these parameter values and estimated the viral kinetic parameters κ_{VSV}, κ_{VV}, δ_{VSV}, δ_{VV}, α_{VSV} and α_{VV} from VSV, VV and VV+VSV treated HT29 tumor growth measurements in ID mice (ie, *HT29/ID-VSV*, *HT29/ID-VV* and *HT29/ID-VV+VSV* obtained by Le Boeuf et al[19]). Then, using IC mice experiments from Rausch et al,[51] we estimated the immune cell-tumor cell contact rate k_p, the immune cell digestion constant $k_{q,s}$, the cytokine production half effect $\Psi_{1/2}$ and the maximal immune cell production rate k_{cp}. To account for the effects of humoral immune responses the viral-kinetic parameters $\omega_{VSV}, \omega_{VV}, \delta_{VSV}, \delta_{VV}$ were then

Figure 1 Schematic representation of the tumor growth model under combination OV-therapy. (A) Biological assumptions for the combination OV-therapy interactions between VV (enhancer) and VSV oncolytic viruses. Infection of cells by either VV or VSV results in cell lysis, whereby new virus particles are released along with a cocktail of antigens, antivirals and cytokines. For simplicity, we considered each virus to release associated cytokines concentrations that can independently instigate the recruitment of immune cells (such as phagocytes). However, in the presence of both VV and VSV infections, we assume the cytokine production decreases the recruitment of immune cells, allowing for a more targeted immune response and virus-induced cell lysis. Additionally, VSV releases antivirals that block the intracellular replication of the virus and the infection of neighboring cells. In comparison, lysis of VV infected cells produces antivirals that downregulate the antivirals produced by VSV, allowing for infection and replication to occur. Once activated, these immune cells induce cell apoptosis of uninfected cancer cells. (B) In the model, quiescent susceptible cells (light blue) activate and begin division by transitioning into the G_1 phase of the cell cycle. Cells exit G_1 to enter the active phase (mitosis) and complete division. Most susceptible cells in the active phase re-enter quiescence after mitosis, however, certain dividing cells may mutate into an immune-resistant lineage (red). Immune interactions are driven by immune cells who encounter quiescent, G_1 and actively dividing susceptible tumor cells. Tumor-immune interactions increase proinflammatory cytokine concentrations to recruit additional immune cells to the tumor site. VSV and VV infect both normal and immune-resistant tumor cells, creating virus-specific infected cell pools. These infected cells undergo lysis releasing new virus progeny. The virus also influences the cytokine production which controls the immune cell production and activity. VSV: vesicular stomatitis virus; VV: vaccinia virus.

recalibrated to the presence of the immune system using 4T1 tumor growth measurements in IC mice under VSV, VV and VV+VSV (ie, *4T1/IC-VSV, 4T1/IC-VV* and *4T1/IC-VV+VSV* obtained by Le Boeuf *et al.*[19]).
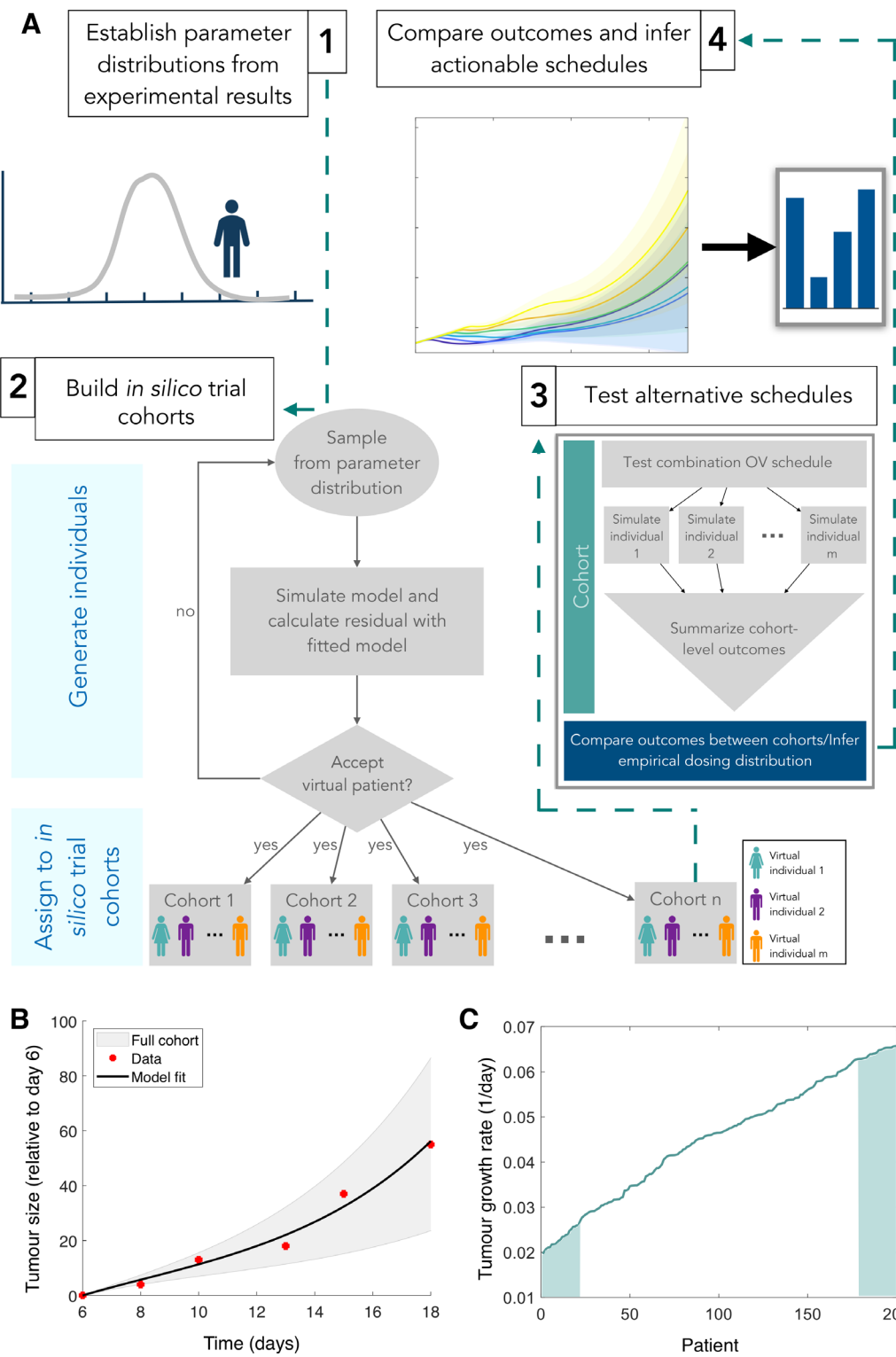
## Generation of in silico individuals and patient cohorts

To reflect interindividual variability and the heterogeneity in treatment outcomes, we generated a unique set of parameters to represent individual virtual patients (figure 2A, no human patients were involved in this study). For this, we sampled tumor and immune cell-related parameters a_1, a_2, d_2, τ, k_p, k_q, k_s, k_{cp} (where τ is the expected tumor cell cycle duration) from a normal distribution with mean μ corresponding to the parameter value returned in the hierarchical fitting described above.

To avoid the inclusion of non-realistic virtual individuals, we verified that each parameter set resulted in a tumor growth within two SD of the experimental measurements and the mean prediction at each corresponding data

time point (figure 2B). Using this approach, we created 200 patients with parameter values normally distributed about the mean empirical or fitted value (online supplemental figure S1, online supplemental information), rejecting 265 parameter sets for not meeting the inclusion criteria. Since the maximal immune cell production rate (k_{cp}) changes when VSV is introduced, we assumed each individual patient's parameter varied equivalently. To recapitulate heterogeneity in initial tumor size and immune populations, we simulated an initial seeding of 10^5 tumor cells, along with an initial cytokine concentration C_0 and immune cell count P_0 (day 0) for each in silico patient parameter set and fixed the initial conditions for treatment to be the tumor and immune populations on day 6 (online supplemental figure S2).

Kaplan-Meier survival curves for each cohort treated using the combination protocols were used to compare the effectiveness of the different trials. To determine a cull threshold for the survival of the virtual patients, we

Figure 2 In silico trial strategy recapitulates experimentally observed variability. (A) (1) Model parameters are established by calibrating experimental results to the model's predictions. A distribution of responses centered at the mean of the experimental data is then used to generate parameter sets representing virtual individuals. (2) To populate the trial, each virtual patient's tumor growth is simulated to determine whether they are candidates for the trial. Patients whose tumor growth is acceptable (ie, clinically relevant) are placed into repeated identical cohorts. (3) Alternative treatment schedules are then tested on each cohort by simulating individual virtual patient responses with the mathematical model and summarizing cohort level outcomes (such as mean and SD of responses). (4) optimal actionable schedules are then inferred by comparing cohort level and individual outcomes. (B) Tumor growth (relative to tumor volume on day 6) over time in absence of treatment. Black line: model fit; red stars: experimental observations measured by Le Boeuf et al,[19] gray shaded region: distribution of growth from full cohort of patients. (C) Virtual patients were ordered based on intrinsic tumor growth rates r (top and bottom 10% denoted by shaded regions). OV: oncolytic virus.

extrapolated the Kaplan-Meier curves in Le Boeuf *et al*[19] by taking populations of 10 randomly sampled individuals and calibrating to their cumulative survival curve, giving a volume threshold (online supplemental technical information, online supplemental figure TS4). A local parameter sensitivity analysis of the mean empirical values showed that tumor growth was closely related to cell cycling rates and immune stimulation (online supplemental figure S3, online supplemental information).

We also quantified the growth rate r of the control tumors by approximating the growth curves with an exponential growth function from day 12 to 18, that is, $r = \left(\ln\left(T\left(18\right) - \ln\left(T\left(12\right)\right)/6\right.$, to obtain an estimate of later tumor growth. This measurement period was chosen to account for the discernable differences between cell lines after day 12 and the experimental end point at day 18.[19] The implicit parameter r describes the aggressivity of the tumors, with high r corresponding to aggressively growing tumors and low r corresponding to slowly growing tumors. Ordering patients by their tumor growth rate showed a gradual increase in r values across the cohort (figure 2C). Numerical simulations, the creation of the virtual cohort, all statistical analyses and figure generation were performed using Matlab R2019b.

RESULTS
Tumor aggressivity dictates the optimal number of enhancer injections

The effect of the multiplicity of VV enhancer injections on the success of therapy is largely unknown, especially for a cohort with varying underlying tumor growth rates. To assess the impact of the number of enhancer administrations, we simulated our virtual cohort after multiple daily enhancer infections followed by a VSV injection given 7 days after the last enhancer (figure 3A). The total number of VV injections (N_E) ranged from 1 to 7 and the dosage sizes were fixed to those used in the Le Boeuf *et al*[19] (online supplemental technical information).

To assess the performance of different enhancer schedules, we quantified the number of tumor cells 15 days after VSV administration (VSV +15 days; figure 3B). In particular, we found that the number of VV enhancers (N_E) did not significantly impact the average tumor size at VSV+15, and that the distribution of tumor sizes between sequential enhancer multiplicities, that is, one enhancer and two enhancers, two enhancers and three enhancers etc., was not significantly different. There was, however, a difference in the distribution of tumor sizes between one enhancer and all other enhancer multiplicities from three enhancers onwards (as confirmed by a Kolmogrov-Smirnov test, $p = 0.0475$, see online supplemental figure S4A for significant pairings). We also determined that the mean number of tumor cells was only significantly different between one and six enhancers, and one and seven enhancers (pairwise t-test, $p = 0.034$ and $p = 3.8 \times 10^{-4}$, respectively; online supplemental figure S4B, online supplemental information). This suggests
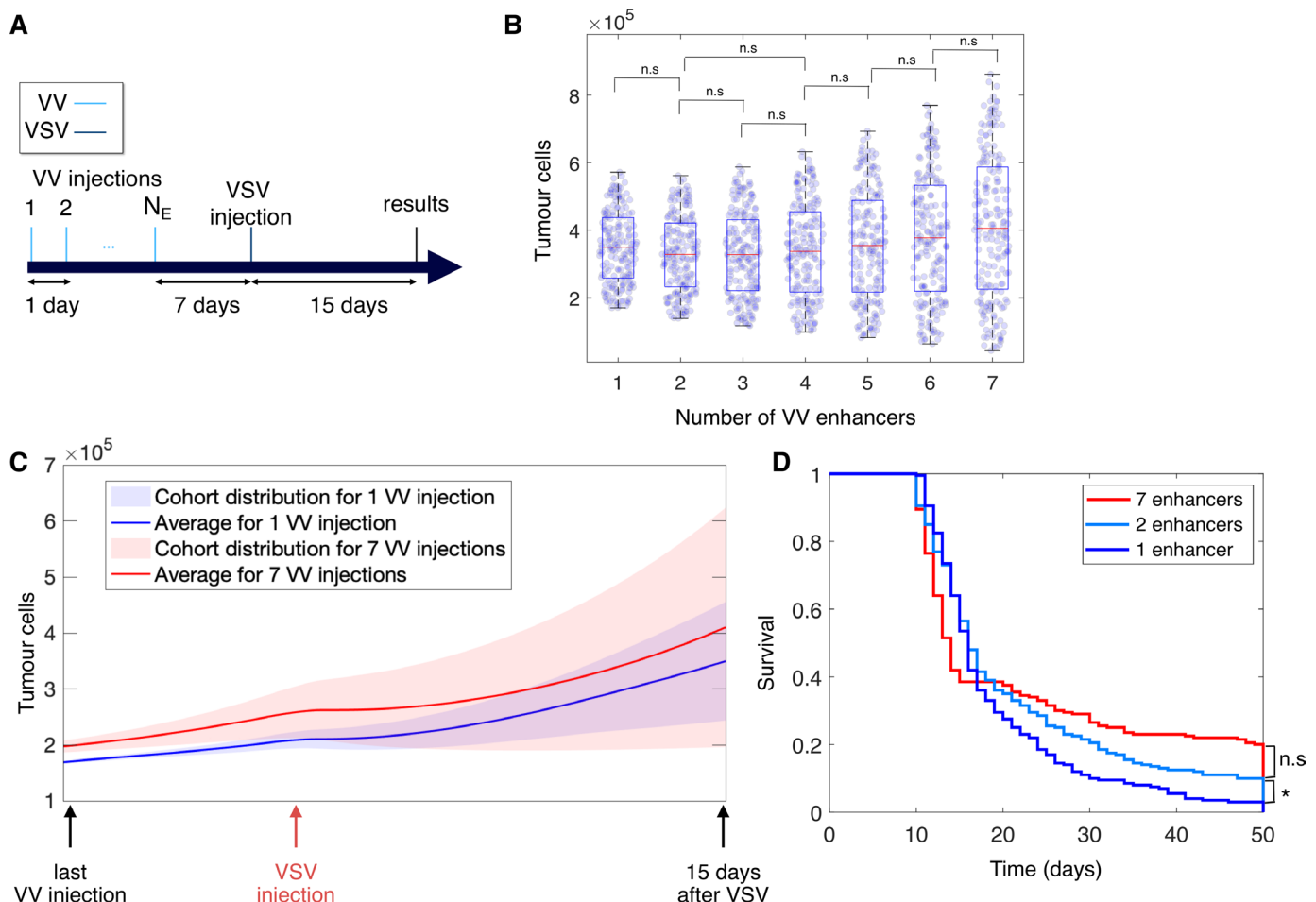
that the duration of treatment and tumor aggressivity could be the principle drivers of the distribution in tumor sizes at 20 days, irrespective of the number of enhancers.

Nonetheless, we were able to distinguish low and high responders by their tumor growth at VSV +15 days after 7 vs 1 enhancer (figure 3C; results for all multiplicities of enhancer injections in online supplemental figure S5A). Though the mean dynamics of the number of tumor cells are qualitatively similar after one or seven enhancers, there is a statistically significant difference in the mean number of tumor cells at VSV +15 days for one enhancer compared with seven enhancers. The difference in variance of cohort responses can be explained by the fact that the last enhancer is administered on day 1 for the one enhancer protocol vs day 6 under the seven enhancer schedule, implying that tumors have ultimately been growing for a longer period of time under the seven enhancer protocol, supporting the conclusion that therapeutic success is largely driven by intrinsic aggressivity (ie, higher growth rates). Log-rank tests of the cohort's Kaplan-Meier survival curves also showed that the one enhancer protocol was significantly different from all others (figure 3D and online supplemental figure S5B in the online supplemental information).
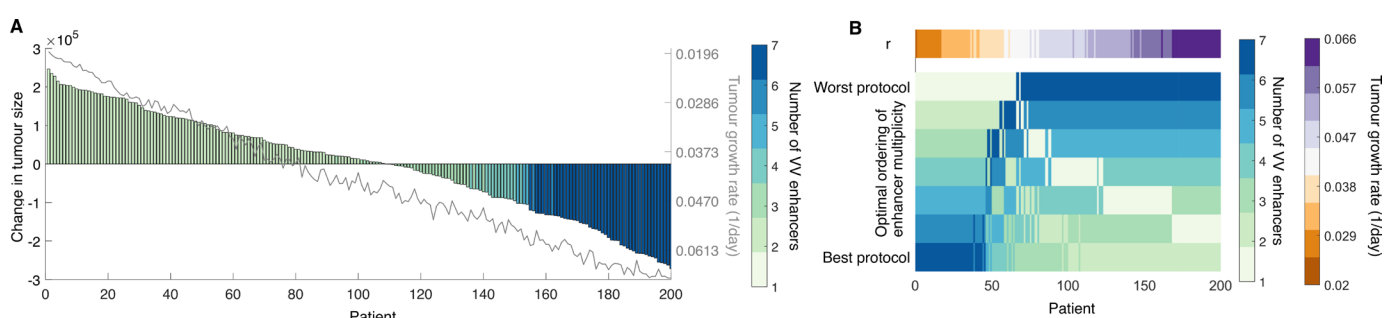
An increase in the variability of responses was observed with a corresponding increase in the number of enhancers (figure 3B). To investigate whether there was a link between a patient's intrinsic tumor growth rate r and the optimal number of enhancers, we established each patient's optimal number of enhancers through numerically simulating all possible treatment protocols and finding the one that minimized tumor burden at VSV +15. We found that the optimal number of enhancers grew with decreases in intrinsic tumor growth rates (figure 4A). Further, our results show that individuals with high growth rates consistently had worse outcomes, even during 'optimal' treatment with two enhancers. To discern patterns of responses in less aggressive tumors and higher growth rates, we ordered the number of enhancers from best protocol to worst protocol for each patient, based on the tumor size 15 days after the VSV injection (figure 4B). Patients with low tumor growth rates were found to perform best under treatment with seven enhancers and worst under treatment with a single enhancer, whereas patients with high tumor growth rates performed best with two enhancers and worst under seven enhancers. These results suggest that there is a significant difference in the efficacy of protocols given a patient's intrinsic tumor growth rate.

Shorter VSV lags are necessary to slow aggressive tumors
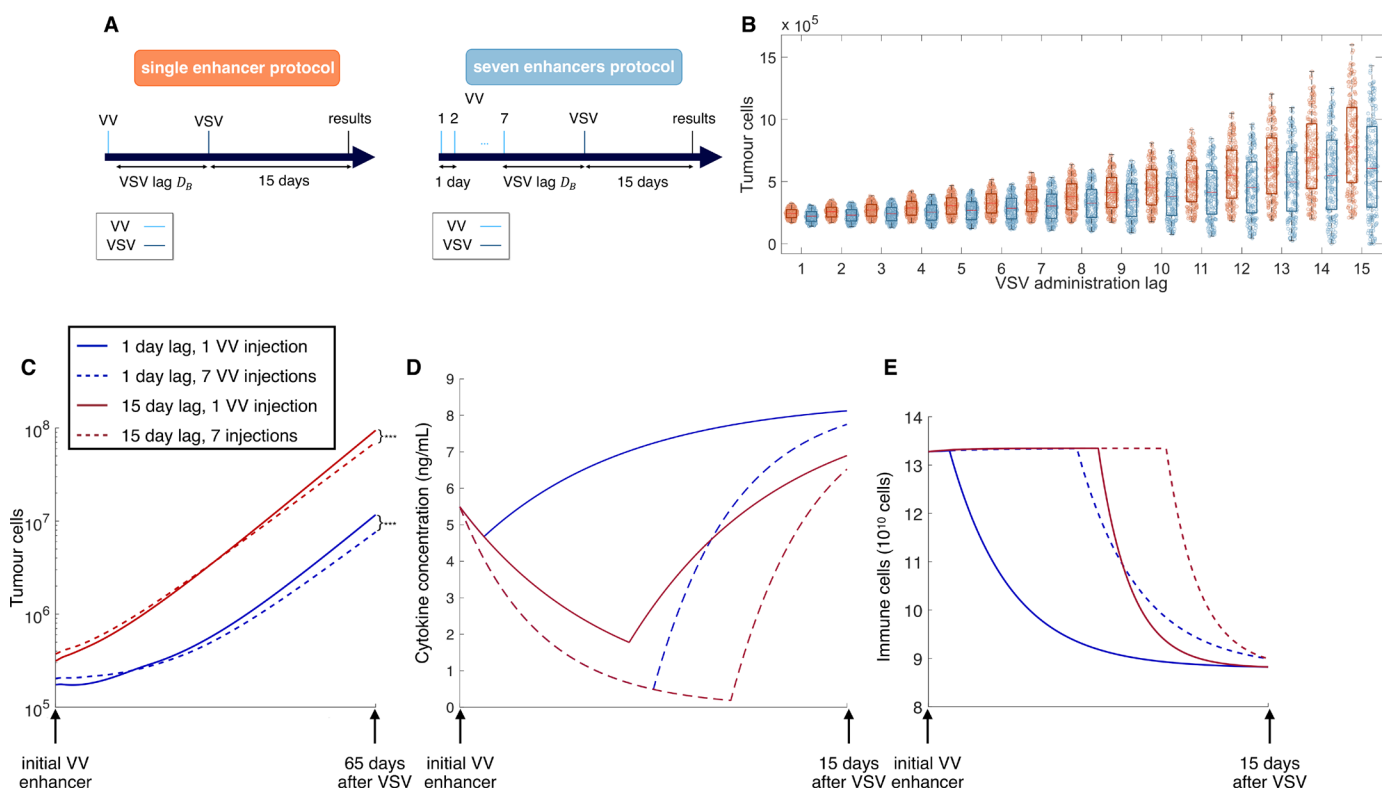
Thus far, enhancer multiplicity was investigated with VSV administered 7 days after the last enhancer. However, the number of days between the final enhancer and the VSV administration can also influence the priming of the immune response and the efficacy of the treatment. To measure the impact of the VSV lag (D_B days), we simulated a single administration of VSV 1–15 days after the

Figure 3 Influence of enhancer injection multiplicity on tumor burden. (A) The effects of enhancer multiplicity (N_E) were investigated by simulating 1–7 VV enhancers, with VSV administered 7 days after the final enhancing dose. Tumor growth was assessed 15 days after the administration of VSV. (B) Distribution in number of tumor cells 15 days after VSV administration with respect to the multiplicity of enhancers. Central mark (red) indicates median, bottom edge denotes the bottom quartile, top edge denotes the top quartile. Significance indicators report the non-significant results of a Kolmogorov-Smirnov test for significance of difference between distributions ($p < 0.05$). (C) Tumor growth dynamics from last enhancer to 15 days after VSV administration for protocols with 1 (blue) and 7 (red) enhancers. Mean is denoted by a solid line, SD by shaded regions of same color and individual virtual patient values are plotted as circles. (D) Kaplan-Meier survival curves for protocols with 1 (dark blue), 2 (light blue) and 7 (red) enhancers. No significant difference between protocols from 2 to 7 enhancers was found (measured by log-rank test for significance, $p < 0.05$). VSV: vesicular stomatitis virus; VV: vaccinia virus.

Figure 4 Individual responses to multiple enhancer injections protocols are stratified by intrinsic tumor growth rates. (A) Waterfall plot of the change in tumor size 15 days after VSV administration. Bar color depicts the optimal number of enhancers. Corresponding tumor growth rate (r) for each patient are plotted in gray. (B) Ordering of protocols from best (bottom row) to worst (top row) for each patient based on the tumor size 15 days after VSV administration. Corresponding tumor growth rates are plotted above (patient ordering identical based on intrinsic tumor growth rate as in A). VSV: vesicular stomatitis virus; VV: vaccinia virus.

Figure 5 Longer VSV lags have a detrimental effect on therapeutic success. (A) Inspired by the results for enhancer multiplicity, the effects of the length of VSV lags were investigated by simulating either a single enhancer protocol (left) or a seven enhancer protocol (right). VSV lags were varied from 1 to 15 days after the final enhancer. Tumor growth was assessed 15 days after the administration of the last VSV. (B) Distribution in number of tumor cells 15 days after VSV administration with respect to the duration of VSV lag after 1 (orange) or 7 (blue) enhancers. Central mark (red) indicates median, bottom edge denotes the bottom quartile, top edge denotes the top quartile and individual virtual patient values are plotted as circles. (C) Tumor growth as a function of time. Markers indicate significant differences in final tumor size (t-test, $p > 0.05$). (D) Cytokine concentrations as a function of time. (E) Immune cells as a function of time. In C, D, E: 1 enhancer, 1-day VSV lag (solid blue), 7 enhancers, 1-day VSV lag (dashed blue), 1 enhancer, 15-day VSV lag (solid red), 7 enhancers, 15-day VSV lag (dashed red). VSV: vesicular stomatitis virus; VV: vaccinia virus.

final enhancer, with dosages fixed as in Le Boeuf *et al*[19] (figure 5A). The number of enhancers was set to either 1 or 7, based on the enhancer multiplicity results described previously. As before, therapeutic response was assessed by the number of tumor cells (ie, tumor size) at VSV +15 days (figure 5B).
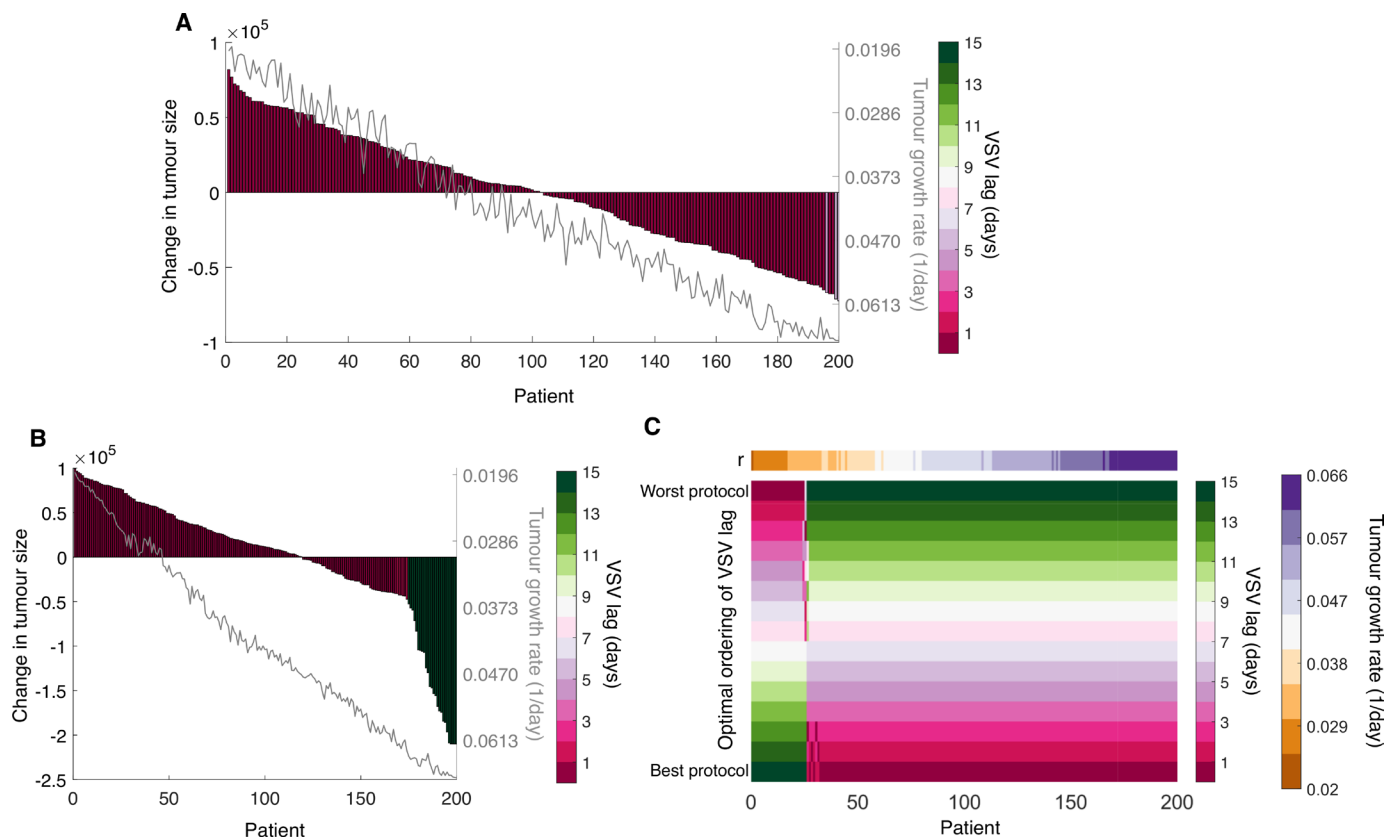
Similar to what was observed with the enhancer multiplicity, increasing the VSV lag increased the variance of the cohort's response (figure 5B). A VSV lag of 1 day, irrespective of the number of enhancers, produced the smallest average tumor size, with a very small distribution of responses at VSV +15 days. In comparison, we observed more dispersion in overall responses for VSV lags of 7 days or more, with some individuals achieving lower tumor sizes than for shorter VSV lags (see online supplemental information, online supplemental figure S6A).

Over longer time, the separation in the tumor size under a 1-day vs 15-day VSV lag becomes clearer (figure 5C). On average, 15-day VSV injection-lags performed the worst of all tested scenarios, especially at longer time points (65 days past VSV). This further solidifies that, as opposed to enhancer multiplicity, the time to VSV administration is the key determinant of tumor size. Since the immune

cell population is essentially stabilized by VSV +15 days (figure 5E), and cytokine concentrations are saturated (figure 5D), the dynamics that occur immediately after the VSV injection must lead to the divergence of long-term tumor behavior.

As we hypothesized that interindividual variability would significantly impact treatment responses, we next investigated the optimal VSV lag for each individual after either one or seven enhancers. For the one enhancer protocol, the optimal VSV lag was a single day for all but three individuals with particularly slow growing tumors, for whom a 5-day VSV lag was best (figure 6A). However, we expect this response to be not particularly significant, as the difference in tumor cell numbers between the optimal and the second most optimal protocol for these three individuals was negligible compared with the rest of the cohort (results not shown).

Tumor responses to treatment were increasingly stratified for optimal schedules after seven enhancer administrations (figure 6B), likely related to the increased interindividual variability observed in this case. We found that optimal schedules for virtual patients with the slowest intrinsic growth rates required a 15-day VSV lag vs

Figure 6 Optimal VSV lag is stratified by intrinsic tumor growth rates. (A) Waterfall plot of the change in tumor size 15 days after the last VSV administration for the one enhancer protocol. Bar color depicts the optimal VSV lag. Corresponding tumor growth rate (r) for each patient are plotted in gray. (B) Waterfall plot of the change in tumor size 15 days after the last VSV administration for the seven enhancer protocol. Bar color depicts the optimal VSV lag. Corresponding tumor growth rate (r) for each patient are plotted in gray. (C) Ordering of protocols from best (bottom row) to worst (top row) for each patient based on the tumor size 15 days after the last VSV administration for seven enhancer protocol. Corresponding tumor growth rates are plotted above (patient ordering identical based on intrinsic tumor growth rate as in B. The ordering of the optimal VSV lag for the one enhancer protocol is provided in online supplemental figure S6 in online supplemental information). VSV: vesicular stomatitis virus.

1 day for those with slow growing tumors. Indeed, there was a clear delineation between aggressively growing tumors that required as short of a lag as possible for maximal therapeutic effect and slower growing tumors that responded best with as long of a VSV lag as possible (figure 6C and online supplemental figure S7 in the online supplemental information). Crucially, individuals with the slowest tumor growth were predicted to have the most meaningful responses, completely recovering in some cases. This again underlines that patient stratification and schedule tailoring is crucial for ensuring the most meaningful clinical response.
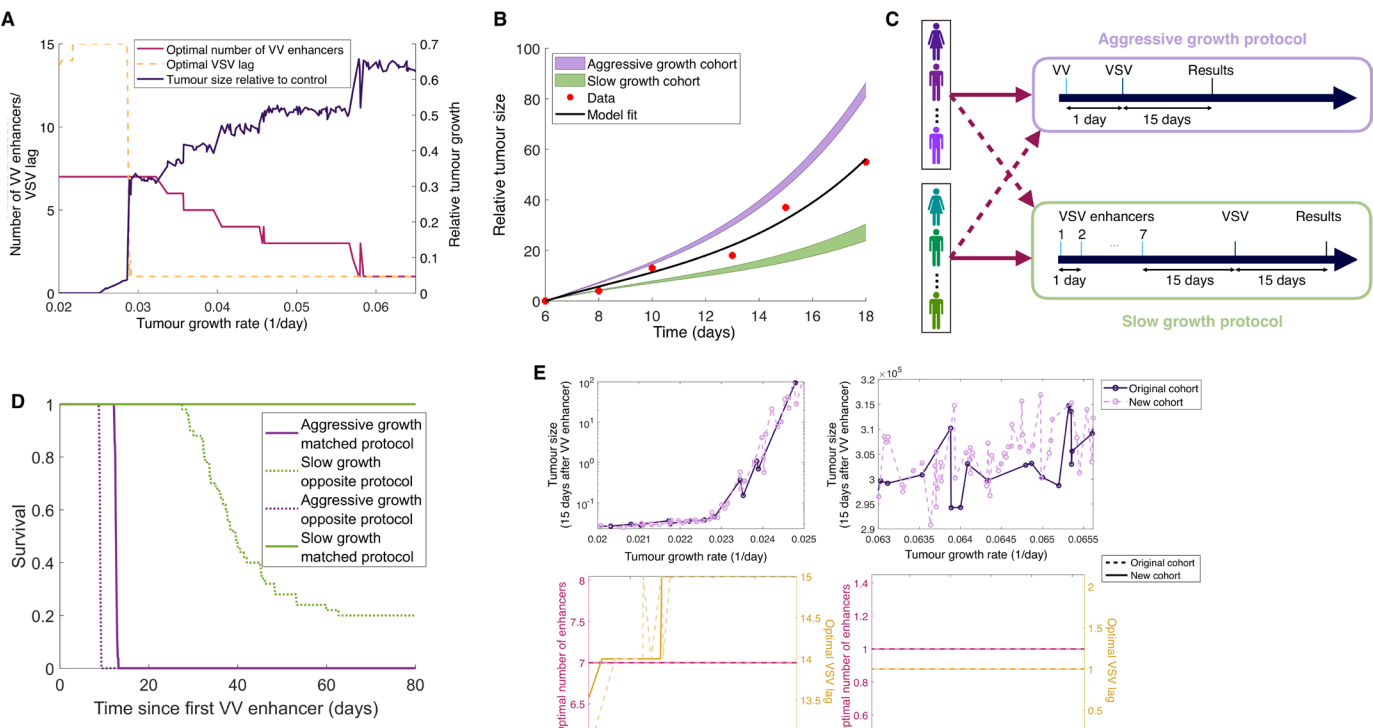
Individualizing enhancer-VSV scheduling

To further delineate vaccination scheduling in distinct subcohorts, we tailored VV enhancer multiplicity (between 1 and 7) and VSV lag (between 1 and 15 days) for each virtual individual according to intrinsic tumor characteristics (figure 7A). The individual optimal protocol was determined by simulating all scheduling possibilities and minimizing tumor size at VSV +15 days.

As before, we found clear stratification between optimal protocols for slowly growing (seven enhancers followed by a 14 or 15 days VSV lag) and fast growing (one enhancer followed by a 1-day VSV lag) tumors (figure 7A). Interestingly, for a range of low intrinsic growth rates r, optimal schedules resulted in near complete tumor removal, whereas we found a jump in the number of tumor cells, followed by a linear dependence on the intrinsic growth rate after a critical value around $r \approx 0.03$ 1/day. Clinically, an r value of 0.03 corresponds to a tumor doubling time of 23 days, which was above the original cohort average of 15 days (figure 2C). Overall, these results underline that tumor aggressivity is the determining factor for combination OV scheduling and the outcome of enhancer-VSV therapy.

Cross-validating tailored strategies

To confirm that outcomes are improved by employing therapeutic strategies based on tumor aggressivity and investigate the robustness of our stratification strategy, we generated two new cohorts comprised of 50 virtual individuals with slow growing tumors ($0.0196 < r < 0.0260$) and

Figure 7 Individualized schedules are determined by tumor aggressivity and risk stratification according to tumor aggressivity is necessary for optimal outcomes. (A) Optimal number of enhancers (yellow), optimal VSV lag (fuchsia) and relative tumor size 15 days after last VSV versus untreated control (purple) as a function of intrinsic tumor growth rate. For all but a subset of the least aggressive tumors, individualized protocols called for a VSV lag of 1 day, with fewer than seven enhancers. (B) Two new cohorts of patients were generated with either aggressive tumor growth ($0.0629 < r < 0.0657$, purple) or slow tumor growth ($0.0196 < r < 0.0260$, green). Original Le Boeuf et al data (red stars) and model fit to the original data (black curve) as in figure 2C. (C) Each cohort was simulated according to the previously determined optimal aggressive protocol (one enhancer followed by a VSV 1 day later) and optimal slow protocol (seven enhancers followed by a VSV 15 days later). To assess the effect specificity of each protocol, a cross-over trial wherein virtual patients with fast growth were treated with the slow protocol and vice versa was performed. (D) Kaplan-Meier survival curves for the two cohorts under the two different protocols. (E) To confirm the robustness of the aggressive and slow protocols, the optimal number of enhancers and VSV lag was then determined for patients in the new cohorts. The results of the newly generated cohort were then compared with the original cohort in A. Tumor size 15 days after the VSV was assessed. Original cohort individualized therapy compared with the new slow growth (top left) and new aggressive growth (top right) individualized schedules. Overlays of the corresponding optimal number of enhancers and VSV lag for each patient from old protocol versus the new slow growth (bottom left) and aggressive growth (bottom right). VSV: vesicular stomatitis virus; VV: vaccinia virus.

50 with aggressively growing tumors ($0.0629 < r < 0.0657$). These ranges for r where chosen to correspond to the top and bottom 10% of the initial cohort's r value (figures 2C and 7B). We next simulated the tumor growth of these cohorts under the previously determined optimal protocols, that is, 7 enhancers and a 15-day VSV lag for slow growing tumors, and one enhancer and a 1-day VSV lag for aggressive tumors (figure 7C). Additionally, we simulated each cohort under the alternate optimal protocol, that is, aggressively growing tumors with the slow tumor growth protocol and vice versa.

Overall, in terms of survival and irrespective of protocol, the aggressive tumor growth cohort performed markedly worse than the slow tumor growth cohort (figure 7D). As these represent the 10% most aggressive tumors of the original cohort, it is not surprising that the efficacy of therapy is minimal. In contrast, survival in the slow growing cohort was markedly different under the two

protocols: when treated with their optimized protocol, all individuals survived, and while survival declined when treated with the aggressive tumor growth protocol, it remained overall stronger than in the aggressive tumor cohort treated with its matched optimal treatment strategy. Nonetheless, both strategies perform better than the no treatment case (results not shown). To further confirm the optimality of the aggressive and slow tumor growth protocols, we also determined each virtual patient's optimized combination schedule for the new cohorts (figure 7E). Unsurprisingly, the optimal protocols were the same as in the larger original cohort, implying there is a robust link between tumor aggressivity and the optimal combination OV-therapy protocol. Interestingly, for patients with extremely slow growing tumors (r close to 0.0196, doubling time of roughly 35 days) the optimal VSV lag was slightly shorter ($D_B = 13$ days) than the rest of the slow growing tumor cohort. Thus, we posit that a

combined OV therapeutic vaccination approach with VV +VSV will be most effective for slow growing tumors.

DISCUSSION

In 2015, the US FDA approved T-VEC for the treatment of non-resectable late-stage melanoma, making it the first OV to reach the Western market. However, despite much promise, the efficacy of OV monotherapy has been limited.[52 53] In response, combined OV schedules hold much promise as an effective cancer therapy capable of eradicating tumor cells through virus infection, immune recruitment, and by providing a long-lasting durable response. Results from combined OV strategies are encouraging, with three clinical trials underway for an adenovirus and OV Maraba anticancer combination OV treatment.[8 9]

A major obstacle to the clinical implementation of combination OV-therapy protocols is designing promising and optimal therapeutic schedules. Further, the reproducibility of protocol efficacy must be demonstrated in heterogeneous patient cohorts. For this preclinical planning, mathematical and computational biology have a large role to play in predicting therapeutic responses and designing effective strategies. Leveraging our previous computational model,[46] we developed an in silico model of combination OV-based therapeutic vaccination with vaccinia (VV) and VSV OVs to test the heterogeneous response to and optimality of an enhancer virus and VSV protocols. Each generated virtual patient was created based on a realistic distribution of model parameters, with growth following the trend of experimental results.

We found that the number of enhancers does not significant impact the average response of our generated virtual cohort. Though perhaps unintuitive, this is likely due to a saturation in the initial immune response. Investigating this further, our results show that while the variance of tumor sizes increased with the number of enhancers, the overall survival of the cohort did not vary significantly. Ultimately, no single optimal protocol was found for most of the cohort. However, at the individual level, there was a significant difference in outcomes found when optimizing the number of enhancers: for tumors with low intrinsic growth rates, a larger number of enhancers is necessary to be effective, whereas aggressive tumors required fewer enhancers. The latter finding supports the idea of 'hitting hard, hitting early' for fast growing tumors. This clear stratification based on tumor aggressivity suggests that the effectiveness of the enhancer-VSV protocol is largely a function of the relationship between viral replication and tumor growth. For a given initial tumor size, faster growing tumors will have more cells for the virus to infect and subsequently lyse, so there is a trade-off between the number of enhancers and the delay in administering the VSV to ensure that cells are sufficiently infected and subsequently recruiting immune cell subsets. On the other hand, for slowly growing tumors, more enhancers are needed to load the tumor microenvironment with

virus and sufficiently activate the immune system. An advantage of OVs compared with other immunostimulatory compounds is that the concentration of OVs in the tumor microenvironment will initially increase due to viral replication, whereas other drugs will experience rapid clearance.

Conceptually, longer VSV lags should increase the mean tumor size, given that tumors are not eradicated by the priming protocol and are thus continuing to grow prior to administration of VSV. Indeed, we predicted that the optimal VSV lag should overall be between 1 and 4 days, or shorter than the currently used 7 days. Similar to what was observed for enhancer multiplicity, we found that increasing the VSV lag increased the dispersion in outcomes, irrespective of the number of enhancers. Thus, it is not necessarily the number of enhancers or VSV lag driving the variation in treatment response, but rather the duration of the treatment.

While there are currently no clinical trials combining VV and VSV for the treatment of TNBC, there are other clinical and experimental results that support the findings of our virtual clinical trial. A handful of clinical trials have been conducted with VV or VSV individually,[9 54–56] and there is currently a phase I trial in stage III-IV melanoma using VSV-IFNbetaTYRP1 (NCT03865212). The randomized phase 2 dose-finding trial of Pexa-Vec (an oncolytic VV with a gene encoded to increase expression of GM-CSF) for the treatment of on advanced hepatocellular carcinoma found a clear distinction in survival based on dosage, with the high-dose cohort having an increase in overall survival compared with the low-dose cohort.[54] Further, the high-dose protocols performed equivalently on patients with or without metastases, whereas, the low dose protocol was only optimal for patients without metastases. As the presence of metastases is an indicator of disease aggressivity, these findings align with our conclusion that the stage and overall aggressiveness of a patient's disease is a determinant for oncolytic VV treatment efficacy, and underlines the importance of patient stratification into appropriate schedules for oncolytic VV therapeutic success.

Further, high levels of Ki-67 expression in TNBC have been found to correlate strongly with more aggressive proliferation and poor prognoses.[57] By evaluating a total of 1800 patients with early invasive TNBC, Zhu *et al*[57] determined that adjuvant chemotherapy was associated with better overall survival in patients with higher Ki-67 expression than patients with low Ki-67 expression, with adjuvant chemotherapy having no effect on disease-free survival in the latter group. Given that Ki-67 is a marker of proliferation, these data corroborate our finding that tumor aggressivity can be a predictor of treatment success in TNBC, and that using Ki-67 expression as a threshold for therapeutic planning and prognostic factor may improve survival.

There are certain limitations to our model formalism. Specifically, the stimulated immune response only impacts the growth of the tumor and only has a secondary

effect on the virus: reducing the number of cells available for the virus to infect and lyse. Despite this shortcoming, our model was able to replicate the observed dynamics of VV and VSV in IC mice and accommodate for the anti-inflammatory and proinflammatory responses to these viruses. Future iterations of the model could build on this and develop a more complex model of the immune response to combination OV-based vaccine therapy. In doing so, our virtual clinical trial platform could be used to optimize combined OV-immunotherapy (such an anti-PD-1 immune checkpoint inhibitor[1]) and investigate whether we see a similar segregation of the optimized protocol based on tumor aggressivity. In addition, future experiments investigating combined VV and VSV treatment in other tumor lines or humans will allow for further model validation.

Through rational considerations, we developed a quantitative approach to therapeutic cancer vaccination that provides actionable and clinically relevant scheduling recommendations that can be easily translated from bench to bedside using complementary methodologies. Current experimental work in therapeutic vaccinations could provide effective novel cancer therapeutics[1 58] and there is a growing push towards personalized tumor-specific vaccination therapies.[59] Unfortunately, the pace of immunotherapy innovation is limited by clinical trial requirements. Here, we put forward a strategy to fill that gap, helping to define the next phase of combined OV regimens.

Author affiliations
[1]Sainte-Justine University Hospital Research Centre, Montreal, Quebec, Canada
[2]Department of Mathematics and Statistics, Université de Montréal, Montreal, Quebec, Canada
[3]Department of Mathematics and Statistics, McGill University, Montreal, Quebec, Canada
[4]Theoretical Biology and Biophysics, Los Alamos National Laboratory, Los Alamos, New Mexico, USA
[5]Statistique et Informatique Décisionnelle, Université Toulouse III Paul Sabatier, Toulouse, Occitanie, France
[6]Institut du Cancer de Montréal, CHUM, Montreal, Quebec, Canada
[7]Department of Microbiology, Infectious diseases and Immunology, Université de Montréal, Montreal, Quebec, Canada

ORCID iDs
Adrianne L Jenner http://orcid.org/0000-0001-9103-7092
Tyler Cassidy http://orcid.org/0000-0003-0757-0017
Morgan Craig http://orcid.org/0000-0003-4852-4770

REFERENCES
1 Ilett E, Kottke T, Thompson J, *et al*. Prime-Boost using separate oncolytic viruses in combination with checkpoint blockade improves anti-tumour therapy. *Gene Ther* 2017;24:21–30.
2 Andtbacka RHI, Kaufman HL, Collichio F, *et al*. Talimogene laherparepvec improves durable response rate in patients with advanced melanoma. *J Clin Oncol* 2015;33:2780–8.
3 Raman SS, Hecht JR, Chan E. Talimogene laherparepvec: review of its mechanism of action and clinical efficacy and safety. *Immunotherapy* 2019;11:705–23.
4 Guo C, Manjili MH, Subjeck JR, *et al*. Therapeutic cancer vaccines: past, present, and future. *Adv Cancer Res* 2013;119:421–75.
5 McGray AJR, Huang R-Y, Battaglia S, *et al*. Oncolytic Maraba virus armed with tumor antigen boosts vaccine priming and reveals diverse therapeutic response patterns when combined with checkpoint blockade in ovarian cancer. *J Immunother Cancer* 2019;7:189.
6 Tysome JR, Li X, Wang S, *et al*. A novel therapeutic regimen to eradicate established solid tumors with an effective induction of tumor-specific immunity. *Clin Cancer Res* 2012;18:6679–89.
7 Bridle BW, Boudreau JE, Lichty BD, *et al*. Vesicular stomatitis virus as a novel cancer vaccine vector to prime antitumor immunity amenable to rapid boosting with adenovirus. *Mol Ther* 2009;17:1814–21.
8 Aitken AS, Roy DG, Martin NT, *et al*. Brief communication; a heterologous oncolytic bacteria-virus prime-boost approach for anticancer vaccination in mice. *Journal of Immunotherapy* 2018;41:125–9.
9 Pol JG, Atherton MJ, Bridle BW, *et al*. Development and applications of oncolytic Maraba virus vaccines. *Oncolytic Virother* 2018;7:117–28.
10 Russell L, Peng KW, Russell SJ, *et al*. Oncolytic viruses: priming time for cancer immunotherapy. *BioDrugs* 2019;33:485–501.
11 Bridle BW, Stephenson KB, Boudreau JE, *et al*. Potentiating cancer immunotherapy using an oncolytic virus. *Mol Ther* 2010;18:1430–9.
12 Bridle BW, Clouthier D, Zhang L, *et al*. Oncolytic vesicular stomatitis virus quantitatively and qualitatively improves primary CD8+ T-cell responses to anticancer vaccines. *Oncoimmunology* 2013;2:e26013.
13 Tysome JR, Li X, Wang S, *et al*. A novel therapeutic regimen to eradicate established solid tumors with an effective induction of tumor-specific immunity. *Clin Cancer Res* 2012;18:6679–89.
14 Martin NT, Roy DG, Workenhe ST, *et al*. Pre-Surgical neoadjuvant oncolytic virotherapy confers protection against rechallenge in a murine model of breast cancer. *Sci Rep* 2019;9:1–6.
15 Li J, O'Malley M, Urban J, *et al*. Chemokine expression from oncolytic vaccinia virus enhances vaccine therapies of cancer. *Mol Ther* 2011;19:650–7.

16 Chisholm RH, Lorenzi T, Clairambault J. Cell population heterogeneity and evolution towards drug resistance in cancer: biological and mathematical assessment, theoretical treatment optimisation. *Biochim Biophys Acta* 2016;1860:2627–45.

17 Stojdl DF, Lichty B, Knowles S, *et al*. Exploiting tumor-specific defects in the interferon pathway with a previously unknown oncolytic virus. *Nat Med* 2000;6:821–5.

18 Arakawa S, Hamami G, Umezu K, *et al*. Clinical trial of attenuated vaccinia virus as strain in the treatment of advanced adenocarcinoma. Report on two cases. *J Cancer Res Clin Oncol* 1987;113:95–8.

19 Le Boeuf F, Diallo J-S, McCart JA, *et al*. Synergistic interaction between oncolytic viruses augments tumor killing. *Mol Ther* 2010;18:888–95.

20 Guse K, Cerullo V, Hemminki A. Oncolytic vaccinia virus for the treatment of cancer. *Expert Opin Biol Ther* 2011;11:595–608.

21 Hastie E, Grdzelishvili VZ. Vesicular stomatitis virus as a flexible platform for oncolytic virotherapy against cancer. *J Gen Virol* 2012;93:2529–45.

22 Bourgeois-Daigneault M-C, Roy DG, Aitken AS, *et al*. Neoadjuvant oncolytic virotherapy before surgery sensitizes triple-negative breast cancer to immune checkpoint therapy. *Sci Transl Med* 2018;10:eaao1641.

23 Urenda-Cázares E, Gallegos A, Macías-Díaz JE. A mathematical model that combines chemotherapy and oncolytic virotherapy as an alternative treatment against a glioma. *J Math Chem* 2020;58:544–54.

24 Abernathy Z, Abernathy K, Stevens J, *et al*. A mathematical model for tumor growth and treatment using virotherapy. *AIMS Math* 2020;5:4136–50.

25 Timalsina A, Tian JP, Wang J. Mathematical and computational modeling for tumor virotherapy with mediated immunity. *Bull Math Biol* 2017;79:1736–58.

26 Lee T, Jenner AL, Kim PS. Application of control theory in a delayed-infection and immune-evading oncolytic virotherapy 2020;17:2361–83.

27 Boemo MA, Byrne HM. Mathematical modelling of a hypoxia-regulated oncolytic virus delivered by tumour-associated macrophages. *J Theor Biol* 2019;461:102–16.

28 Simbawa E, Al-Johani N, Al-Tuwairqi S. Modeling the spatiotemporal dynamics of oncolytic viruses and radiotherapy as a treatment for cancer. *Comput Math Methods Med* 2020;2020:1–10.

29 Haghnegahdar A, Zhao J, Feng Y. Lung aerosol dynamics of airborne influenza A virus-laden droplets and the resultant immune system responses: an in silico study. *J Aerosol Sci* 2019;134:34–55.

30 Elaiw AM, Al Agha AD. A reaction–diffusion model for oncolytic M1 virotherapy with distributed delays. *Eur. Phys. J. Plus* 2020;135:117.

31 Jenner A, Yun C-O, Yoon A, *et al*. Modelling heterogeneity in viral-tumour dynamics: the effects of gene-attenuation on viral characteristics. *J Theor Biol* 2018;454:41–52.

32 Villasana M, Radunskaya A. A delay differential equation model for tumor growth. *J Math Biol* 2003;47:270–94.

33 Barish S, Ochs MF, Sontag ED, *et al*. Evaluating optimal therapy robustness by virtual expansion of a sample population, with a case study in cancer immunotherapy. *Proc Natl Acad Sci U S A* 2017;114:E6277–86.

34 Castiglione F, Mantile F, De Berardinis P, *et al*. How the interval between prime and boost injection affects the immune response in a computational model of the immune system. *Comput Math Methods Med* 2012;2012:1–9.

35 Peterson MC, Riggs MM. FDA Advisory meeting clinical pharmacology review utilizes a quantitative systems pharmacology (QSP) model: a watershed moment? *CPT Pharmacometrics Syst Pharmacol* 2015;4:189–92.

36 Alfonso S, Jenner AL, Craig M. Translational approaches to treating dynamical diseases through in silico clinical trials. *Chaos* 2020;30:123128.

37 Boem F. Silico clinical trials: a possible response to complexity in pharmacology. *Uncertainty in Pharmacology* 2020:135–52.

38 Gkouskou K, Vlastos I, Karkalousos P. The "Virtual Digital Twins" Concept in Precision Nutrition. *Adv Nutr* 2020.

39 Vittinghoff E, McCulloch CE, Woo C, *et al*. Estimating long-term effects of treatment from placebo-controlled trials with an extension period, using virtual twins. *Stat Med* 2010;29:1127–36.

40 Schmidt BJ, Casey FP, Paterson T, *et al*. Alternate virtual populations elucidate the type I interferon signature predictive of the response to rituximab in rheumatoid arthritis. *BMC Bioinformatics* 2013;14:221.

41 Agur Z. From the evolution of toxin resistance to virtual clinical trials: the role of mathematical models in oncology. *Future Oncology* 2010;6:917–27.

42 Allen RJ, Rieger TR, Musante CJ. Efficient generation and selection of virtual populations in quantitative systems pharmacology models. *CPT Pharmacometrics Syst Pharmacol* 2016;5:140–6.

43 Wang H, Milberg O, Bartelink IH, *et al*. *In silico* simulation of a clinical trial with anti-CTLA-4 and anti-PD-L1 immunotherapies in metastatic breast cancer using a systems pharmacology model. *R Soc Open Sci* 2019;6:190366.

44 Yin Z, Huynh JM, Liu G. Designing combination therapies with modeling chaperoned machine learning 2019:1–17.

45 Pérez-García VM, Ayala-Hernández LE, Belmonte-Beitia J, *et al*. Computational design of improved standardized chemotherapy protocols for grade II oligodendrogliomas. *PLoS Comput Biol* 2019;15:e1006778–17.

46 Cassidy T, Craig M. Determinants of combination GM-CSF immunotherapy and oncolytic virotherapy success identified through in silico treatment personalization. *PLoS Comput Biol* 2019;15:e1007495.

47 Cassidy T, Humphries AR. A mathematical model of viral oncology as an immuno-oncology instigator. *Math Med Biol* 2020;37:117–51.

48 Jafarnejad M, Gong C, Gabrielson E, *et al*. A computational model of neoadjuvant PD-1 inhibition in non-small cell lung cancer. *Aaps J* 2019;21:79.

49 Milberg O, Gong C, Jafarnejad M, *et al*. A QSP model for predicting clinical responses to monotherapy, combination and sequential therapy following CTLA-4, PD-1, and PD-L1 checkpoint blockade. *Sci Rep* 2019;9:1–17.

50 Marshall HD, Urban SL, Welsh RM. Virus-Induced transient immune suppression and the inhibition of T cell proliferation by type I interferon. *J Virol* 2011;85:5929–39.

51 Rausch MP, Hahn T, Ramanathapuram L, *et al*. An orally active small molecule TGF-beta receptor I antagonist inhibits the growth of metastatic murine breast cancer. *Anticancer Res* 2009;29:2099–109.

52 Marelli G, Howells A, Lemoine NR, *et al*. Oncolytic viral therapy and the immune system: a double-edged sword against cancer. *Front Immunol* 2018;9:1–8.

53 Chesney J, Puzanov I, Collichio F, *et al*. Randomized, open-label phase II study evaluating the efficacy and safety of talimogene laherparepvec in combination with ipilimumab versus ipilimumab alone in patients with advanced, unresectable melanoma. *J Clin Oncol* 2018;36:1658–67.

54 Heo J, Reid T, Ruo L, *et al*. Randomized dose-finding clinical trial of oncolytic immunotherapeutic vaccinia JX-594 in liver cancer. *Nat Med* 2013;19:329–36.

55 Zeh HJ, Downs-Canner S, McCart JA, *et al*. First-In-Man study of Western reserve strain oncolytic vaccinia virus: safety, systemic spread, and antitumor activity. *Mol Ther* 2015;23:202–14.

56 Breitbach CJ, Parato K, Burke J, *et al*. Pexa-Vec double agent engineered vaccinia: oncolytic and active immunotherapeutic. *Curr Opin Virol* 2015;13:49–54.

57 Zhu X, Chen L, Huang B, *et al*. The prognostic and predictive potential of Ki-67 in triple-negative breast cancer. *Sci Rep* 2020;10:1–10.

58 Mougel A, Terme M, Tanchot C. Therapeutic cancer vaccine and combinations with antiangiogenic therapies and immune checkpoint blockade. *Front Immunol* 2019;10:467.

59 Hu Z, Ott PA, Wu CJ. Towards personalized, tumour-specific, therapeutic vaccines for cancer. *Nat Rev Immunol* 2018;18:168–82.

Supplementary Information: In silico trials predict that combination strategies for enhancing vesicular stomatitis oncolytic virus are determined by tumour aggressivity

Authors: Adrianne L. Jenner, Tyler Cassidy, Katia Belaid, Marie-Claude Bourgeois-Daigneault, Morgan Craig

Correspondence to :

morgan.craig@umontreal.ca

This PDF file includes:

Supplementary Results
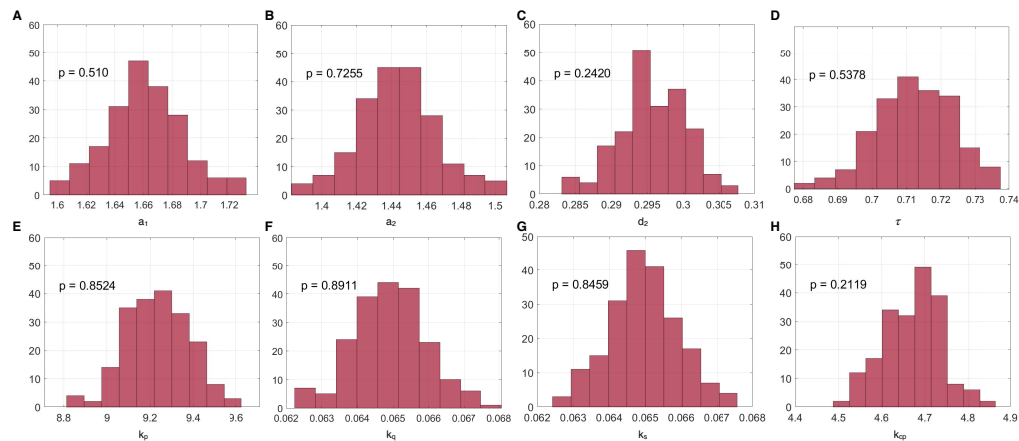
Figs. S1 to S5

References: 1
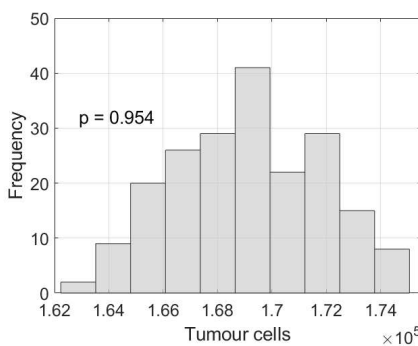
SUPPLEMENTARY RESULTS

Virtual individuals parameter distributions

Parameter sets for the *in silico* trial were drawn from normal distributions centered at the fixed values of the 4T1-VV+VSV immune model (Table TS3-TS4). The model was then simulated for each parameter set, and only those virtual individuals whose tumour growth were within two standard deviations of the standard error reported in the data from the experiments were retained in the *in silico* trial. All parameter distributions were confirmed to be normally distributed using the Shapiro-Wilk test[1,2] (Fig. S1). A histogram of the initial number of tumour cells across the cohort is provided in Fig. S2, p-values indicate the results of a Shapiro-Wilk test of normality.

Figure S1. Distribution for the parameter values in the in silico trial. A)-H) *The distribution for the parameters* $a_1, a_2, d_2, \tau, k_p, k_q, k_s, k_{cp}$. *The p-value returned from the Shapiro-Wilk test of normality for each distribution is indicated on the corresponding plots. p-values greater than 0.05 imply that we cannot reject the null-hypothesis of no statistically significant difference between the parameter and normal distributions.*
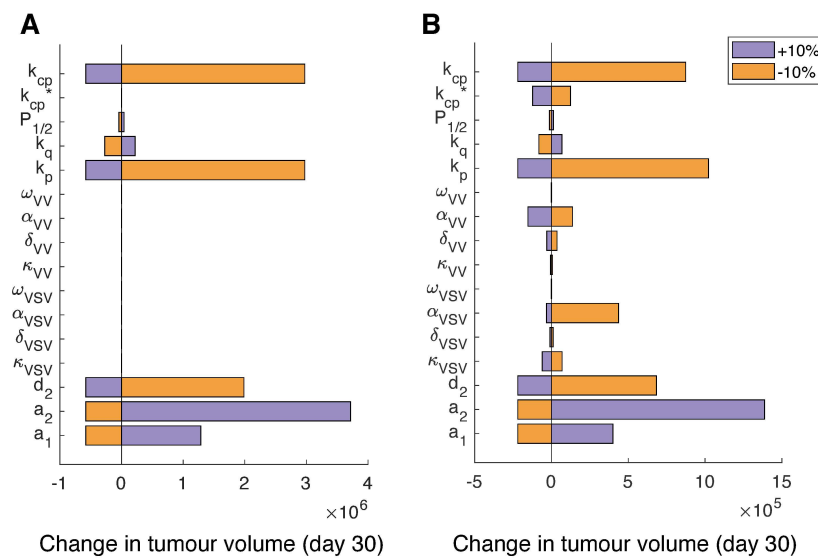
Figure S2. Distribution of the total initial number of tumour cells for the cohort (200 virtual patients) at the start of treatment (day 0). Patient-specific initial conditions were determined by seeding each virtual patient's initial tumour with 10^5 cells and simulating the computational model until day 6, p-value reports the outcome of the Shapiro-Wilk test for normality.

Sensitivity of tumour growth in 4T1-VV+VSV immune model

We investigated the sensitivity of each of the parameters fit to the 4T1 tumour growth (*4T1/IC*) in immunocompetent (IC) mice (see Technical Supplementary Information) by perturbing their values $\pm 10\%$ (Fig. S3A) and found parameters relating tumour growth to rate cells transit from interphase to active phase (a_2), and immune related parameters including the immune cell-tumour cell contact rate k_p and the maximal immune cell production rate k_{cp} to be the most locally sensitive. This suggests that a stronger immune cell response to the presence of tumour cells can result in natural tumour eradication without treatment which is consistent with the analytical study of the model[3]. Complete tumour eradication was also achieved through manipulating parameters for the cell cycle a_1 and a_2 and the death of quiescent cells d_2.
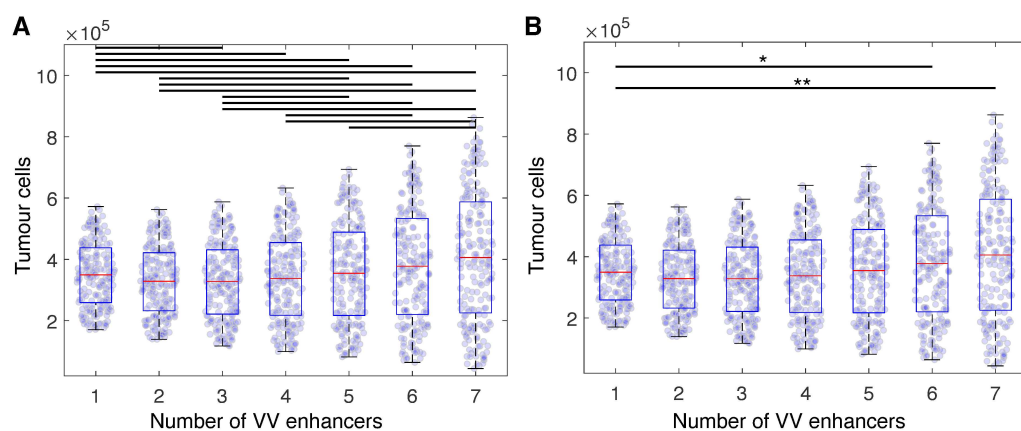
In the case of fits to 4T1 tumour growth under VV and VSV treatment (*4T1/IC-VV+VSV*), the same parameters a_2, k_p and k_{cp} were again found to be most sensitive (Fig. S3B), suggesting that the underlying tumour growth and immune involvement are major determinants of the treatment outcome, and that viral characteristics are less important. The sensitivity to a_2 is likely due to the fact that cells in the G_1 phase of the model have a constant death rate, so the longer or shorter that they spend in G_1 will impact the number of cells that survive that phase of the cell cycle and go on to reproduce.

3

Figure S3. Parameter sensitivity results. *Tornado plot of parameter sensitivity in A) 4T1/IC model (control tumour growth) and B) the 4T1/IC-VV+VSV model (consecutive injections of VV and VSV in 4T1 tumour immunocompetent model). Each parameter was varied by $\pm 10\%$ and the resulting change in the tumour volume on day 20 was recorded. Purple bars correspond to an increase of 10% and orange bars correspond to a decrease of 10%.*

Tests for significance in the enhancer-multiplicity protocols
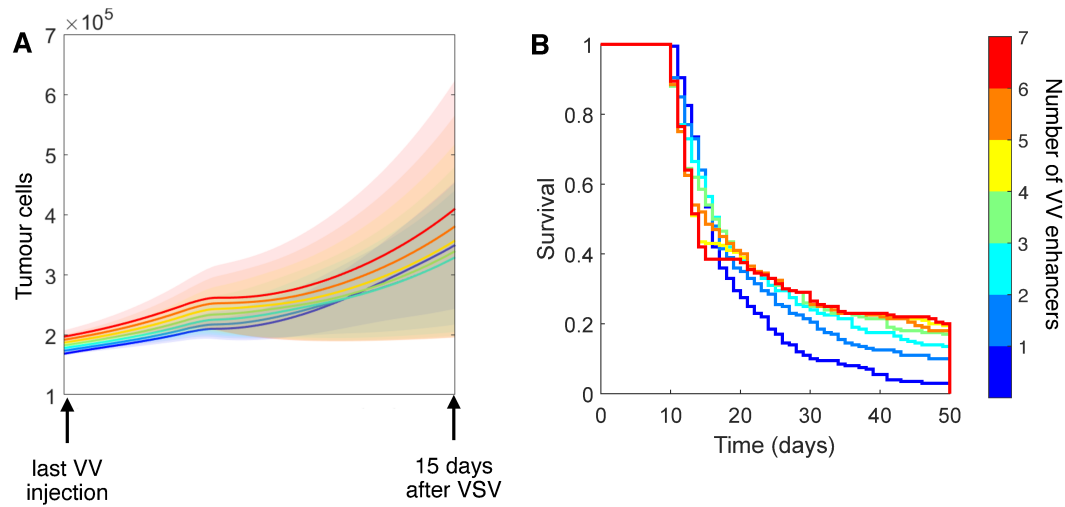
The Kolmogorov-Smirnov test, which assesses whether two arbitrary distributions are the same, was used to evaluate the significance between cohort tumour cell numbers after different protocols. The Matlab function *kstest2* was used to test the null hypothesis that the data were from the same continuous distribution (Fig. S4).

Supplemental material

BMJ Publishing Group Limited (BMJ) disclaims all liability and responsibility arising from any reliance placed on this supplemental material which has been supplied by the author(s)

J Immunother Cancer

Figure S4. Significance results for the enhancer multiplicity trial. *Tumour growth for the cohort of patients was simulated for 1 to 7 enhancers with a VSV 7 days after the last enhancer. The number of tumour cells was measured for each individual in the cohort 15 days after the VSV. A) Results of the Kolmogorov-Smirnov test for significance, where the significant pairings have been noted ($p < 0.05$). B) Result of a two sample t-test, where the significant pairings have been noted. The bar for significance represents the two sample t-test. The test returned a significant p-value 0.005<p*<0.05 and p**<0.0005 for one enhancer and all other enhancers.*

Full results for the enhancer multiplicity investigation

The temporal dynamics for all enhancer multiplicities considered (extension of Fig. 4C in the text) and the survival for the cohort under all enhancer multiplicities considered (extension of Fig. 4D) are provided in Figs. S5A and S5B, respectively.

Figure S5. Influence of enhancer multiplicity on tumour growth. *Complementary results to Fig. 4 in Main Text. A) The effects of enhancer multiplicity were investigated by simulating 1-7 enhancers, with a VSV administered 7 days after the final priming dose (statistical significances found in Fig. S4A). Tumour growth was assessed 15 days after the administration of the VSV. B) Kaplan-Meier survival curves for all enhancer multiplicities.*
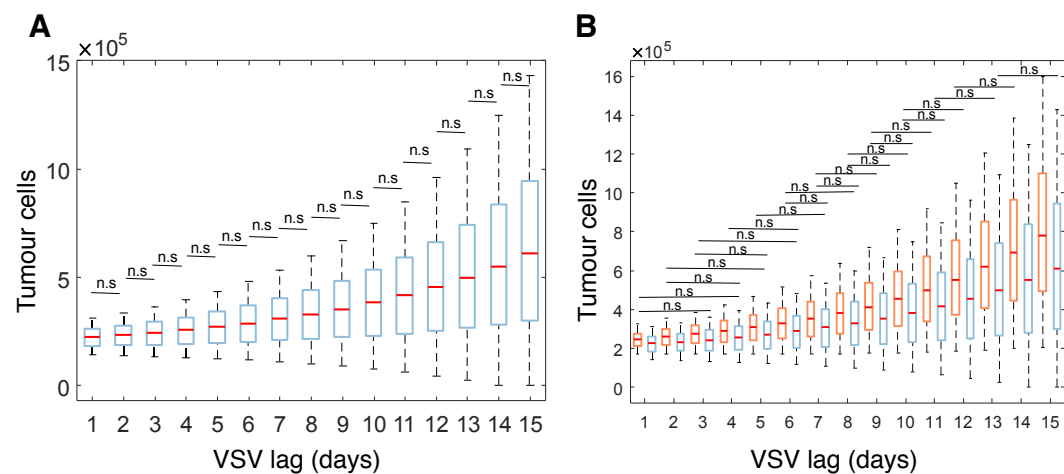
Tests for significance in the VSV-lag protocols

A two-sample t-test was used to determine whether there was significant difference in the mean outcome for the cohorts under different VSV lags (from 1 day to 15 days). All means were

5

Supplemental material

BMJ Publishing Group Limited (BMJ) disclaims all liability and responsibility arising from any reliance
placed on this supplemental material which has been supplied by the author(s)

J Immunother Cancer

significantly different for the VSV lag protocols with 1 enhancer. For 7 enhancer VSV lag protocols, a VSV lag of n days and $n + 1$ days was found to not be significant (Fig. S6A). On average, cohort responses were statistically significant for the 1 enhancer VSV-lag protocols (pairwise T-test, $p < 0.05$), whereas we found consecutive VSV lags of n and $n + 1$ days were not statistically significant (pairwise T-test, $p < 0.05$) for the 7 enhancer VSV-lag protocols. Comparing the 1 enhancer and 7 enhancer VSV-lag protocols we found that 1 enhancer protocols with n day VSV-lag and 7 enhancers with an $n + 2$ day VSV-lag were not significantly different (pairwise T-test, $p < 0.05$, Fig. S6B), which suggests that equivalent average responses from a 1 enhancer protocol could be obtained with a 7-enhancer protocol by extending the VSV lag by 2 ± 1 days.
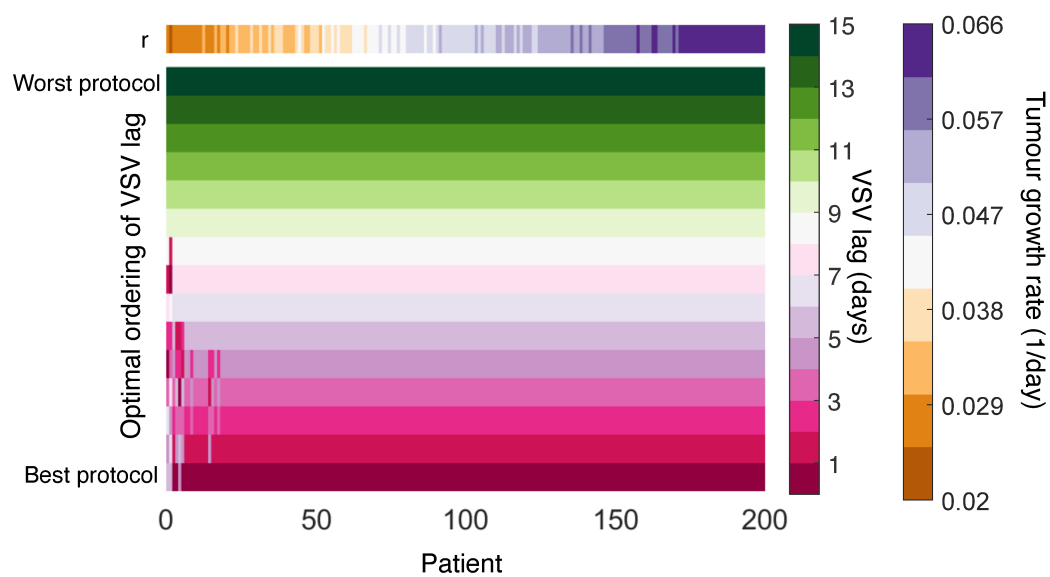
Order of optimal VSV lag for the 1 enhancer protocol

For each patient, the VSV lags from 1 day to 15 days were ordered from most optimal to least optimal based on the tumour size obtained 15 days after the last VSV given only a single enhancer (Fig. S7). Most patients had an optimal VSV lag of 1 day and a least optimal VSV lag of 15 days, implying that it is best to administer the VSV as soon as possible, if only administering a single enhancer. For some patients who had low tumour growth rates r, the optimal VSV lag was 7 days. Overall, for all patients, the least optimal VSV lag was 15 days.

Figure S6. Significance of VSV lag. *A) Results of the two-sample t-test for significance for the 7 enhancer VSV-lag trial, where the non-significant pairings have been noted. The test returns a significant p-value <0.05.*

6

B) Non-significant pairings of 1 enhancer (orange) and 7-enhancer (blue) VSV-lag protocols comparisons. All other pairings were significant.

Figure S7. Optimal VSV lag for 1 enhancer protocol. *Ordering of protocols from best (bottom row) to worst (top row) for each patient based on the tumour size 15 days after the last VSV administration for 7 enhancer protocol. Corresponding tumour growth rates are plotted above (patient ordering identical based on intrinsic tumour growth rate as in Fig. 7A in the Main Text.*

REFERENCES

1   Shapiro SS, Wilk MB. An analysis of variance test for normality (complete samples). *Biometrika* 1965;**52**:591–611.

2   Öner M, Deveci Kocakoç Ipek. Jmasm 49: A compilation of some popular goodness of fit tests for normal distribution: Their algorithms and MATLAB codes (MATLAB). *J Mod Appl Stat Methods* 2017;**16**:30.

3   Cassidy T, Humphries AR. A mathematical model of viral oncology as an immuno-oncology instigator. *Math Med Biol A J IMA* 2020;**37**:117–151. doi:10.1093/imammb/dqz008

Supplemental material

BMJ Publishing Group Limited (BMJ) disclaims all liability and responsibility arising from any reliance placed on this supplemental material which has been supplied by the author(s)

J Immunother Cancer

Technical Supplementary Information: In silico trials predict that combination strategies for enhancing vesicular stomatitis oncolytic virus are determined by tumour aggressivity

Authors: Adrianne L. Jenner, Tyler Cassidy, Katia Belaid, Marie-Claude Bourgeois-Daigneault,

Morgan Craig

Correspondence to :

morgan.craig@umontreal.ca

This PDF file includes:

Methods

Supplementary Analysis

Figs. TS1 to TS4

Tables S1 to S3

References 1 to 14

1

METHODS

Mathematical model of combination OV-based therapeutic vaccination

The computational model's formalism was based on Cassidy and Humphries[1], with parameterization as in Cassidy and Craig[2], who determined optimized treatment schedules for combined T-VEC and GM-CSF. This model explicitly accounts for heterogeneity in tumour cell cycle time and tumour-immune interactions through a distributed delay differential equation, and describes the quiescent tumour cell population ($Q(t)$), and the G1-phase tumour cell population ($G_1(t)$) with the remainder of mitosis described as a delayed process with a delay kernel $K(t)$ representing the duration of the mitotic portion of the cell cycle. We assumed that the cell cycle duration is Erlang distributed as was done by Cassidy and Craig[2], but other distributions are also possible[1,3,4].

As described in the main text, we have expanded the model described in Cassidy and Craig[2] to include vaccinia (VV) and vesicular stomatitis virus (VSV) viral strains, $V_{VV}(t)$ and $V_{VSV}(t)$, and associated viral dynamics. This includes the introduction of virus-specific rates for the virion to cell infection rate, κ_{VSV} and κ_{VV}; the cell lysis rate, δ_{VSV} and δ_{VV}; the lytic virion burst size, α_{VSV} and α_{VV}; and the virion death rate, ω_{VSV} and ω_{VV}. Similarly, the model now includes a VV-infected cell population, $I_{VV}(t)$, and a VSV-infected cell population, $I_{VSV}(t)$. Pro-inflammatory cytokines, $C(t)$, are produced in response to the presence of uninfected and infected tumour cells. Immune cells, $P(t)$, are recruited to the tumour site by the cytokine concentration and are able to kill uninfected tumour cells. We consider $P(t)$ to represent the overall average response of the immune system and includes the action of macrophages, T cells and other phagocytes. The complete model is given by

$$\frac{d}{dt}Q(t) = 2(1-\mu)\int_{-\infty}^{t} exp\left[-\int_{\sigma}^{t}\hat{d}_K + \kappa_{VV}\eta(V_{VV}(x)) + \kappa_{VSV}\eta(V_{VSV}(x)) + \psi_G(U(x))dx\right] a_2 G_1(\sigma)K(t-\sigma)d\sigma - [a_1 + d_1 + \psi_Q(U(t))]Q(t)$$

$$\frac{d}{dt}G_1(t) = a_1 Q(t) - [a_2 + d_2 + \kappa_{VV}\eta(V_{VV}(t)) + \kappa_{VSV}\eta(V_{VSV}(t)) + \psi_G(U(t))]G_1(t),$$

2

$$\frac{d}{dt}Q_R(t) = 2\mu \int_{-\infty}^{t} \exp\left[-\int_{\sigma}^{t} \hat{d}_K + \kappa_{VV}\eta(V_{VV}(x)) + \kappa_{VSV}\eta(V_{VSV}(x)) + \psi_G(U(x))dx\right] a_2 G_1(\sigma)K(t-\sigma)d\sigma$$

$$+ 2\int_{-\infty}^{t} \exp\left[-\int_{\sigma}^{t} \hat{d}_K + \kappa_{VV}\eta(V_{VV}(x)) + \kappa_{VSV}\eta(V_{VSV}(x))dx\right] a_2 G_{1,R}(\sigma)K(t-\sigma)d\sigma$$

$$- [a_1 + d_1]Q_R(t),$$

$$\frac{d}{dt}G_{1,R}(t) = a_1 Q_R(t) - [a_2 + d_2 + \kappa_{VV}\eta(V_{VV}(t)) + \kappa_{VSV}\eta(V_{VSV}(t))]G_{1,R}(t),$$

$$\frac{d}{dt}I_{VSV}(t) = \kappa_{VSV}\eta(V_{VSV}(t))[G_1(t) + G_{1,R}(t) + N(t) + N_R(t)] - \delta_{VSV}I_{VSV}(t),$$

$$\frac{d}{dt}I_{VV}(t) = \kappa_{VV}\eta(V_{VV}(t))[G_1(t) + G_{1,R}(t) + N(t) + N_R(t)] - \delta_{VV}I_{VV}(t),$$

$$\frac{d}{dt}V_{VSV}(t) = -\kappa_{VSV}\eta(V_{VSV}(t))[G_1(t) + G_{1,R}(t) + N(t) + N_R(t)] + \alpha_{VSV}\delta_{VSV}I_{VSV}(t) - \omega_{VSV}V_{VSV}(t),$$

$$\frac{d}{dt}V_{VV}(t) = -\kappa_{VV}\eta(V_{VV}(t))[G_1(t) + G_{1,R}(t) + N(t) + N_R(t)] + \alpha_{VV}\delta_{VV}I_{VV}(t) - \omega_{VV}V_{VV}(t),$$

$$\frac{d}{dt}C(t) = C_{prod}(U(t)) - k_{elim}C(t),$$

$$\frac{d}{dt}P(t) = \phi(C(t)) - \gamma_p P(t),$$

$$I(t) = I_{VSV}(t) + I_{VV}(t),$$

$$V(t) = V_{VSV}(t) + V_{VV}(t).$$

All other parameters are in Cassidy and Craig[2]. To simplify notation in the functions $\eta(U(t)), \psi_Q(U(t)), \psi_G(U(t)), \phi(C(t))$, and $C_{prod}(U(t))$ described below, we introduce

$$U(t) = [Q(t), G_1(t), I(t), V(t), C(t), P(t)].$$

Phagocytosis of quiescent and mitotic tumour cells was considered to occur at respective rates

$$\psi_Q(U(t))Q(t) = \frac{k_p P(t)}{1 + k_Q Q(t)}Q(t),$$

and

$$\psi_G(U(t))G_1(t) = \frac{k_p P(t)}{1 + k_s G_1(t)}G_1(t).$$

The infection of susceptible cells by the oncolytic virus was modelled by

$$\eta(V(t)) = \frac{V(t)}{\eta_{1/2} + V(t)}.$$

3

Immune cells are recruited to the tumour microenvironment by the inflammatory cytokines at a rate of

$$\phi\big(C(t)\big) = \frac{k_{cp}C(t)}{C_{1/2}+C(t)},$$

and inflammatory cytokines are produced at rate

$$C_{prod}\big(U(t)\big) = C_{prod}^* + \rho\big(C_{prod}^{max} - C_{prod}^*\big)\frac{\delta I + \Psi\big(U(t)\big)}{\Psi_{\frac{1}{2}} + \delta I + \Psi\big(U(t)\big)},$$

where

$$\Psi\big(U(t)\big) = \psi_G(P,G_1)G_1 + \psi_Q(P,Q)Q = \frac{k_pP(t)}{1+k_sG_1(t)}\big(G_1(t)+N(t)\big) + \frac{k_pP(t)}{1+k_qQ(t)}Q(t).$$

An anti-inflammatory state can be caused by cells releasing anti-inflammatory cytokines such as interleukin-10 (IL-10) or transforming growth factor β (TGF-β)[5] after viral infection. Further, infection by virus can also cause a reduction in the production of pro-inflammatory cytokines, e.g. interleukin-12 (IL-12), that are necessary to support a strong anti-viral immune response[5]. In contrast, a pro- inflammatory response is instigated when a virus-infected cell activates immune cells through cytokine signaling. These activated immune cells release pro-inflammatory immune-stimulatory cytokines, such as IL-12 and IL-2[6–8], that aid in the recruitment and proliferation of immune cells. The ability of viruses to instigate a pro- or anti-inflammatory immune response depends on the type of virus. As mentioned in the main text, to model the immune response, we introduced an inflammatory modulation parameter (ρ) into the production rate of inflammatory cytokines $C_{prod}\big(U(t)\big)$ where $0 \leq \rho \leq 1$. Cytokine production from infected cells and cycling tumour cells is decreased for small values of ρ, simulating an anti-inflammatory response.

The total number of non-resistant and resistant cells in the cell cycle, $N(t)$ and $N_R(t)$ respectively, is thus given by

$$N(t) = \int_0^\infty a_2 \exp\left[-\int_{t-\xi}^t \hat{d}_K + \kappa_{VV}\eta\big(V_{VV}(x)\big) + \kappa_{VSV}\eta\big(V_{VSV}(x)\big) + \psi_G\big(U(x)\big)dx\right]\left(1 - \int_0^\xi K(\sigma)d\sigma\right)G_1(t-\xi)d\xi,$$

and

4

$$N_R(t) = \int_0^\infty a_2 \exp\left[-\int_{t-\xi}^t \hat{d}_K + \kappa_{VV}\eta(V_{VV}(x)) + \kappa_{VSV}\eta(V_{VSV}(x))dx\right]\left(1 - \int_0^\xi K(\sigma)d\sigma\right)G_{1,R}(t-\xi)\,d\xi.$$

The total number of tumour cells $T(t)$ at any point in time t is calculated by

$$T(t) = Q(t) + G_1(t) + N(t) + Q_R(t) + G_{1,R}(t) + N_R(t) + I_{VV}(t) + I_{VSV}(t).$$

Intravenous administration of oncolytic viruses was modelled by

$$Dose_V(t) = \sum_{j=1}^N \frac{k_a^v F_v Admin_i^v(t)}{Vol}\exp\left(-k_a^v(t - t_j)\right),$$

where $Dose_j^v$ is the amount of virus administered at time $t = t_j$ and

$$Admin_j^v(t) = \begin{cases} 0 & \text{if } t < t_j, \\ Dose_j^v & \text{if } t \geq t_j, \end{cases}$$

similar to the formalism in Cassidy and Craig[2].

To numerically solve the full model, we applied the linear chain technique to replace the distributed delay term by the solution of a system of linear ODEs and reduce the system to an equivalent finite dimensional system of ODEs[1–3]. This reduction now explicitly depends on the shape and scale parameters, k_{tr} and j, that arise from the parametrization of the Erlang distribution kernel $K(t)$[2]. The transformed system of ODEs is given by

$$\frac{dQ(t)}{dt} = 2(1-\mu)k_{tr}A_j(t) - a_1Q(t) - d_1Q(t) - \psi_Q(U(t))Q(t),$$

$$\frac{dG_1(t)}{dt} = a_1Q(t) - \left[a_2 + d_2 + \kappa_{VV}\eta(V_{VV}(t)) + \kappa_{VSV}\eta(V_{VSV}(t)) + \psi_G(U(t))\right]G_1(t),$$

$$\frac{dA_1(t)}{dt} = a_2G_1(t) - k_{tr}A_1(t) - \left(\hat{d}_g + \kappa_{VV}\eta(V_{VV}(t)) + \kappa_{VSV}\eta(V_{VSV}(t)) + \psi_G(U(t))\right)A_1(t),$$

$$\frac{dA_i(t)}{dt} = k_{tr}(A_{i-1}(t) - A_i(t)) - \left(\hat{d}_g + \kappa_{VV}\eta(V_{VV}(t)) + \kappa_{VSV}\eta(V_{VSV}(t)) + \psi_G(U(t))\right)A_i(t),$$

$$\text{for } i = 2,3,\dots,j$$

$$\frac{dQ_R(t)}{dt} = 2\mu k_{tr}A_j(t) + 2k_{tr}A_{j,R}(t) - a_1Q_R(t) - d_1Q_R(t),$$

$$\frac{dG_{1,R}(t)}{dt} = a_1Q_R(t) - a_2G_{1,R}(t) - d_2G_{1,R}(t) - \left(\kappa_{VV}\eta(V_{VV}(t)) + \kappa_{VSV}\eta(V_{VSV}(t))\right)G_{1,R}(t),$$

5

Supplemental material

BMJ Publishing Group Limited (BMJ) disclaims all liability and responsibility arising from any reliance placed on this supplemental material which has been supplied by the author(s)

J Immunother Cancer

$$\frac{dA_{1,R}(t)}{dt} = a_2 G_{1,R}(t) - k_{tr}A_{1,R}(t) - \left(\hat{d}_g + \kappa_{VV}\eta(V_{VV}(t)) + \kappa_{VSV}\eta(V_{VSV}(t)) + \psi_G(U(t))\right)A_{1,R}(t),$$

$$\frac{dA_{i,R}(t)}{dt} = k_{tr}\left(A_{i-1,R}(t) - A_{i,R}(t)\right) - \left(\hat{d}_g + \kappa_{VV}\eta(V_{VV}(t)) + \kappa_{VSV}\eta(V_{VSV}(t)) + \psi_G(U(t))\right)A_{i,R}(t),$$

$$\text{for } i = 2,3,\dots,j,$$

$$\frac{dI_{VV}(t)}{dt} = \kappa_{VV}\eta(V_{VV}(t))\left[G_1(t) + G_{1,R}(t) + N(t) + N_R(t)\right] - \delta_{VV}I_{VV}(t),$$

$$\frac{dI_{VSV}(t)}{dt} = \kappa_{VSV}\eta(V_{VSV}(t))\left[G_1(t) + G_{1,R}(t) + N(t) + N_R(t)\right] - \delta_{VSV}I_{VSV}(t),$$

$$\frac{dV_{VV}(t)}{dt} = \alpha_{VV}\delta_{VV}I_{VV}(t) - \omega_{VV}V_{VV}(t) - \kappa_{VV}\eta(V_{VV}(t))(G_1(t) + N(t)),$$

$$\frac{dV_{VSV}(t)}{dt} = \alpha_{VSV}\delta_{VSV}I_{VSV}(t) - \omega_{VSV}V_{VSV}(t) - \kappa_{VSV}\eta(V_{VSV}(t))(G_1(t) + N(t)),$$

$$\frac{dC(t)}{dt} = C_{prod}(U(t)) - k_{elim}C(t),$$

$$\frac{dP(t)}{dt} = \phi(C(t)) - \gamma_p P(t)$$

with initial conditions carefully chosen to ensure that the solution of the finite dimensional system above defined a solution of the infinite dimensional distributed DDE model[1,2]. The initial conditions for the cytokine and immune cells (C_0 and P_0 respectively) were determined by solving P and C at homeostasis, i.e. setting $dP/dt = dC/dt = 0$. The variables in the model are summarized in Table TS1, with values obtained during fitting in Table TS2 and then final parameter values in Table TS3-TS4.

6

Supplemental material

BMJ Publishing Group Limited (BMJ) disclaims all liability and responsibility arising from any reliance placed on this supplemental material which has been supplied by the author(s)

J Immunother Cancer

Parameter	Units	Description
$Q(t)$	cells	Quiescent tumour cells
$G_1(t)$	cells	G1-phase tumour cells
$Q_R(t)$	cells	Resistant quiescent tumour cells
$G_{1,R}(t)$	cells	Resistant G1-phase tumour cells
$I_{VSV}(t)$	cells	Tumour cells infected by VSV
$I_{VV}(t)$	cells	Tumour cells infected by VV
$I(t)$	cells	Total infected cell population
$V_{VSV}(t)$	virions	Vesicular stomatitis virus (VSV) free virus
$V_{VV}(t)$	virions	Vaccinia (VV) free virus
$V(t)$	virions	Total virus
$C(t)$	ng/mL	Cytokine concentration
$P(t)$	10^{10}cells	Immune cells
$N(t)$	Cells	The total number of non-resistant tumour cells in the cell cycle
$N_R(t)$	Cells	The total number of resistant tumour cells in the cell cycle

Table TS1. Summary of variables in the model.

7

Supplemental material

BMJ Publishing Group Limited (BMJ) disclaims all liability and responsibility arising from any reliance placed on this supplemental material which has been supplied by the author(s)

J Immunother Cancer

Experimental measurements used to estimate VV and VSV related viral and immune parameters

To estimate the parameters in the model, we used a hierarchical fitting algorithm where subsets of the model were fit to different experiments using VV and VSV in immunodeficient and immunocompetent mice to allow for individual aspects of a given biological interaction to be understood in isolation. For example, we leveraged experiments in immunodeficient mice to fit parameters in the model relating solely to tumour growth. These parameters were then fixed when fitting the immune-related parameters to data from immunocompetent mice. Using this approach, we reduce the degrees of freedom at each stage of parameter fitting and obtain more reliable estimates for individual parameter values.

Two primary data sources were leveraged. Le Boeuf *et al.*[9] measured the relative tumour volume in immunodeficient and immunocompetent mice after treatment with VV and VSV. Tumours were established using the HT29 (human colorectal adenocarcinoma) cell line in immunodeficient mice with an initial injection of 3×10^6 cells. After 10 days, they tested three treatment protocols on the these tumours: a single intravenous injection of VSV (1×10^7 pfu), a single intravenous injection of VV (1×10^6 pfu), and a single intravenous injection of VV (1×10^6 pfu) followed two days later by a single intravenous injection of VSV (1×10^7 pfu). Cell line 4T1 (breast cancer) tumours were then established in immunocompetent mice using an initial injection of 1×10^5 cells. After 6 days, they tested three treatment protocols: using a single intravenous injection of VSV (1×10^8 pfu), a single intravenous injection of VV (1×10^7 pfu), and a single intravenous injection of VV (1×10^7 pfu) followed two days later by a single intravenous injection of VSV (1×10^8 pfu). The relative tumour volume $\tilde{T}(t,\hat{t})$ on day t relative to day $\hat{t}$ i.e.

$$\tilde{T}(t,\hat{t}) = \frac{T(t) - T(\hat{t})}{T(\hat{t})} \times 100, \qquad (1)$$

was monitored for ten mice in each protocol for each cell line and then averaged for each experiment. In Eq. (1), $T(t)$ is the tumour volume on day t, and is used to calculate the relative tumour volume $\tilde{T}(t,\hat{t})$, also known also as a relative index[10,11].

8

We also incorporated 4T1 tumour growth measurements in immunodeficient and immunocompetent mice from Rausch *et al.*[12]. Here, tumour growth was reported in area (mm^2) as opposed to in volume (mm^3) as in Le Boeuf *et al*. We therefore converted Rausch *et al.*'s tumour area measurements to tumour volume by assuming the tumours were spherical. We also converted both sets of data to a measurement for the number of cells by assuming that $1\ mm^3$ contains 1×10^6 cells[2,13]. The nine experiments considered are summarized below:

- *HT29/ID* **-** HT29 cell tumour growth in an immune-deficient mouse model
- *4T1/ID* – 4T1 cell tumour growth in an immune-deficient mouse model
- *HT29/ID-VSV* – HT29 cell tumour growth under VSV treatment in immune-deficient mouse model
- *HT29/ID-VV* – HT29 cell tumour growth under VV treatment in immune-deficient mouse model
- *HT29/ID-VV+VSV* – HT29 cell tumour growth under VV and VSV treatment (administered sequentially) in immune-deficient mouse model
- *4T1/IC* – 4T1 cell tumour growth in immune-competent mouse model
- *4T1/IC-VSV* – 4T1 cell tumour growth under VSV treatment in immune-competent mouse model
- *4T1/IC-VV* – 4T1 cell tumour growth under VV treatment in immune-competent mouse model
- *4T1/IC-VV+VSV* – 4T1 cell tumour growth under VV and VSV treatment (administered sequentially) in immune-competent mouse model

Overview of fitting algorithm for VV and VSV related viral and immune parameters

We conducted a sequential fit of the experimental measurements digitized from Le Boeuf *et al.*[9] and Rausch *et al.*[12] to estimate viral and immune related parameters. At each step of the fitting algorithm, any parameters that were either not being estimated or had not been previously determined, were fixed to the value determined by Cassidy and Craig[2] (Table TS2).

9

First, tumour growth parameters were obtained by fitting the parameters a_1, a_2 and d_2 by minimizing the square difference between the average tumour growth measurements and the corresponding model simulation from both the HT29 and 4T1 cell lines in immunodeficient mice (i.e. *HT29/ID* and *4T1/ID*). Then, fixing these parameter values for the HT29 tumour growth, we used the VSV and VV and treated HT29 tumour growth measurements in immunodeficient mice (i.e. *HT29/ID-VSV* and *HT29/ID-VV*) to obtain the virus-specific kinetic parameters κ_{VSV}, κ_{VV}, δ_{VSV}, δ_{VV}, $\alpha_{VSV}, \alpha_{VV}$. As mentioned in the main text, we assumed that VV and VSV would have specific infection rates (κ_{VV} and κ_{VSV}), lysis rates (δ_{VV} and δ_{VSV}), and total virions created through lysis (α_{VV} and α_{VSV})[9].

VV inhibits the production of antiviral factors (such as type 1 interferons) that normally decrease the speed of VSV spread through reducing infectivity and affecting viral production[9]. Thus, we assumed for the experiment in nude mice where VV and VSV are administered sequentially (i.e. *HT29/ID-VV+VSV*), VV would first prime the local tumour environment so that VSV's ability to lyse cells was enhanced, hence the name enhancer. Biologically, we assumed that the reduction in the presence of type I IFN allows for more viral replication leading to faster lysing of infected cells[14]. As such, the lysis rate of VSV-infected cells, δ_{VSV}, would increase in the *HT29/ID-VV+VSV* experiment compared to the previous experiment with VSV alone (i.e. *HT29/ID-VSV*). Additionally, since the multiplicity of infection (MOI) for a virus can be affected by the introduction of a second virus, and MOI can have an impact on replication and lytic properties of viruses[15], we assumed that the lysis rate of VSV infected cells may vary between the single injection of VSV alone and VSV injected after VV was already present. We also assumed all other viral kinetic parameters (κ_{VSV}, κ_{VV}, δ_{VV}, α_{VSV} and α_{VV}) would be the same for the combined virus experiment (i.e. *HT29/ID-VV+VSV*) as the individual virus experiments (*HT29/ID-VV* and *HT29/ID-VSV*).

Immune parameters $k_p, k_{s,q}$ and $\Psi_{1/2}$ were next obtained using the 4T1 tumour growth in an immunocompetent model (*4T1/IC*). Then, to fit the 4T1 tumour growth under VV and VSV treatment (i.e. *4T1/IC-VV* and *4T1/IC-VSV*), we hypothesized that the lysis rates of each virus, δ_{VV} and δ_{VSV}, would vary according to the specific cell line (i.e. HT29 vs 4T1) but the virion infection rate, κ_{VV} and

10
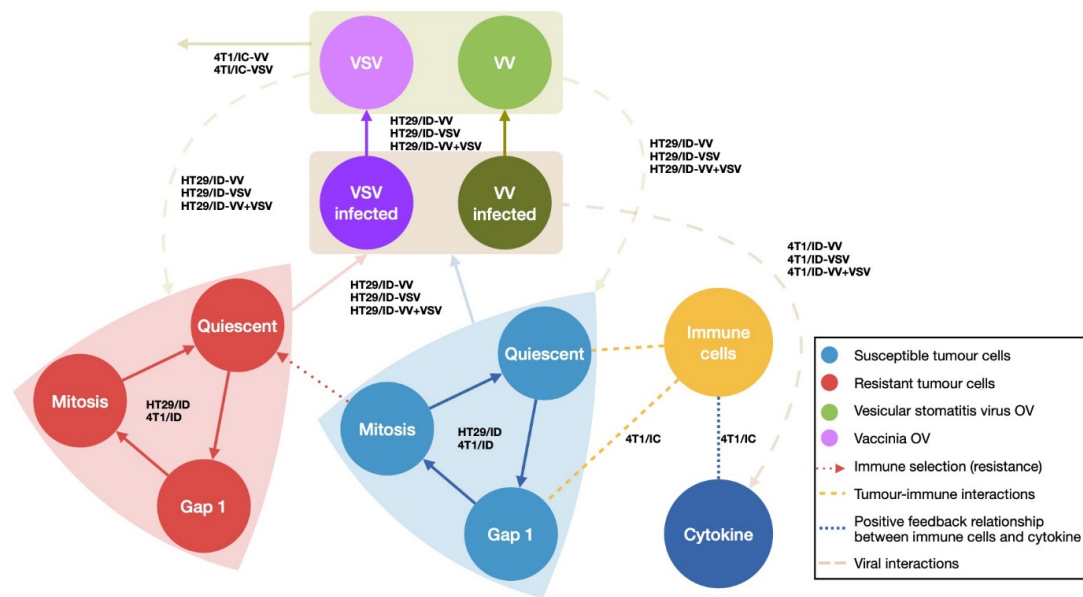
κ_{VSV}, and the lytic virion burst size, α_{VSV} and α_{VV}, would be conserved. This assumption is based on the belief that virion-cell infection rates will not be significantly affected by the underlying tumour cell type and that the lytic virion burst size would primarily depend on the virus type as opposed to the cell-type. This assumption is supported by observed differences in the length of the eclipse phase for VV (8-10 hours[16]) and VSV (~3 hours[17]), their rates of plaque generation, and overall viral loads[9,18]. The *4T1/IC-VV* and *4T1/IC-VSV* experiments were also used to fit the virion decay rates, ω_{VSV} and ω_{VV}, as we expected these rates to be higher after injection into an immunocompetent mouse.

Since VV reduces the production of antiviral factors[9], we fixed $\rho = 0$ to simulate an anti-inflammatory response was initiated when VV was introduced, and allowed $\rho = 1$ for VSV to reflect its inflammatory properties when administered without VV[9]. In the immunocompetent mouse model where VV and VSV were administered sequentially (*4T1/IC-VV+VSV*), we also assumed that the injection of VSV after VV commenced replication would decrease the maximal immune cell production rate k_{cp}. As elevated cytokine production would increase phagocytosis of cells, ultimately reducing the VSV-infection and subsequent cell lysis, a decrease in k_{cp} would result in an increase in the lysis of VSV-infected cells. To model this effect, we therefore reduced k_{cp}. Additionally, the reduction in immune cell production could be a result of cytokine receptors on virus-specific immune cell binding limited amounts of growth-factors, and competing with newly developing immune cell responses[5] (such as for the VSV infection).

Although the viral kinetic parameters were predominantly estimated using measurement for HT29 tumour growth, we assumed that any impact on viral dynamics of changing to the 4T1 tumour cell line is accounted for by the change in tumour growth parameters between the HT29 and 4T1 cell lines (a_1, a_2, d_2), and also through the variation in lytic burst rate δ_{VSV} and δ_{VV} (Table TS2). In addition, the Le Boeuf et al.[9] experiments measured each virus individually then in combination, providing a more accurate estimation of differences in VV and VSV viral parameters through fitting the tumour growth under either virus individually.

Fig. 1 (Main Text) is a schematic representation of the dynamics occurring in the model for the *4T1/IC-VV+VSV* experiment. Since our model considers only a singular pro-inflammatory cytokine

11

population and immune compartment, the complex immune network occurring in the VV and VSV

treatment had to be simplified. A summary of the fitting procedure for all model parameters is provided

in Fig. TS1.

Figure TS1. Hierarchical fitting scheme. *To estimate the parameters in the model, 9 different data sets were*

used: HT29/ID, HT29/ID-VV, HT29/ID-VSV, HT29/ID-VV+VSV, 4T1/IC, 4T1/IC-VV, 4T1/IC-VSV and 4T1/IC-

VV+VSV from Le Boeuf et al.[9] *and 4T1/ID from Rausch et al.*[12]*. Each of these data sets was used to fit*

parameters for a specific interaction between the sensitive (blue) and resistant (red) uninfected tumour cells, the

sensitive and resistant infected (dark purple and dark green) tumour cells, the virus (dark purple and dark

green) and the cytokines (dark blue) and immune cells (yellow). Names of the data set overlaid on the related

interaction indicates data sets used to obtain parameters.

At each step, parameter estimates were obtained by calculating model predictions from the stiff

ODE solver *ode15s* in Matlab R2019b and using the nonlinear least squares fitting algorithm *lsqnonlin*

via the trust-region-reflective algorithm to estimate parameters that fit model predictions to the data.

The termination tolerance was 10^{-6}, the maximum number of function evaluations was fixed as

$100 \times$ the number of parameters, and the maximum number of iterations for each fit was 400. Multiple

initial seeds were used to confirm that the optimal parameters were obtained. Alternate reduced

parameter sets were attempted for the fit of the different data sets, however, the only way to capture the

data was to allow for heterogeneity in the tumour-virus interactions as described in detail above and summarized in Table TS2.

SUPPLEMENTAL RESULTS

Parameter estimates

The initial number of cells for each model simulation was fixed to the corresponding value used in the experiment, or the extrapolation from a $10mm^2$ area to volume, as described above. The values of a_1, a_2 and d_2 for *HT29/ID* and *4T1/ID* tumours were then fitted, with a lower bound for a_2 obtained based on the intermitotic time for cervical cancer cells and the observation that the mean duration of phases S-G$_2$-M is strictly positive[2], i.e. $\tau = 1.40 - 1/a_2$ and $\tau > 0$. As these mice were immunodeficient, the immune response was ignored and we set $Q_R(t) = G_{1,R}(t) = N_R(t) = P(t) = C(t) = 0$. Additionally, as there was no virus present in the control experiments, $I(t) = V(t) = 0$ (see Fig. TS2A and TS2B, and Tables TS2 and TS3).

Fixing the HT29 tumour growth parameters for the immunodeficient mouse model, the viral-kinetic parameters were obtained by fitting to the *HT29/ID-VV* and *HT29/ID-VSV* experiments, where at $t = 11$ days, a single dose of either VV or VSV was administered. The size of the virus injection was scaled by 10^5 to avoid any computational stiffness of the model. For the dual-dose experiment *HT29/ID-VV+VSV*, VSV was administered two days after the initial dose of VV. As these experiments were also conducted in nude mice, the immune response was negligible, i.e. $Q_R(t) = G_{1,R}(t) = N_R(t) = C(t) = P(t) = 0$. The *HT29/ID-VV*, *HT29/ID-VSV* and *HT29/ID-VV+VSV* experiments were fit simultaneously (see Jenner *et al.*[13] for more details on simultaneously fitting). The results of these fits are provided in Fig. TS2C-TS2E and Tables TS2 and TS3.

Fixing the 4T1 tumour growth parameters obtained for *4T1/ID*, the *4T1/IC* measurements, we next estimated the immune kinetic parameters $k_p, k_{q,s}$ and $\Psi_{1/2}$ (Fig. TS2F and Table TS2). The virus was then recalibrated to the 4T1 tumour cells and the immune presence by fitting $\delta_{VV}, \delta_{VSV}, \omega_{VV}$ and ω_{VSV} to the *4T1/IC-VV* and *4T1/IC-VSV* experiments (Fig. TS2G and TSH). The immune modulation

13

Supplemental material

BMJ Publishing Group Limited (BMJ) disclaims all liability and responsibility arising from any reliance placed on this supplemental material which has been supplied by the author(s)

J Immunother Cancer

parameter ρ was fixed to represent the inflammatory and anti-inflammatory capabilities of VV and VSV, respectively.

As discussed above, we hypothesized in the *HT29/ID-VV+VSV* model that the synergism between VV and VSV would alter the lysis rate of the secondary virus (VSV), and we kept this assumption for the immunocompetent equivalent experiment. We also assumed that the injection of VSV into a tumour immune-competent environment after VV commenced replication would further down-regulate the phagocyte production by cytokines at the tumour site, increasing the lysis rate of VSV particles in turn. Therefore, we introduced the piecewise conditions:

$$\rho = \begin{cases} 1 & t < N_E - 1 \\ 0 & N_E - 1 \leq t < N_E - 1 + D_B \\ p^* & t \geq N_E - 1 + D_B \end{cases}$$

and
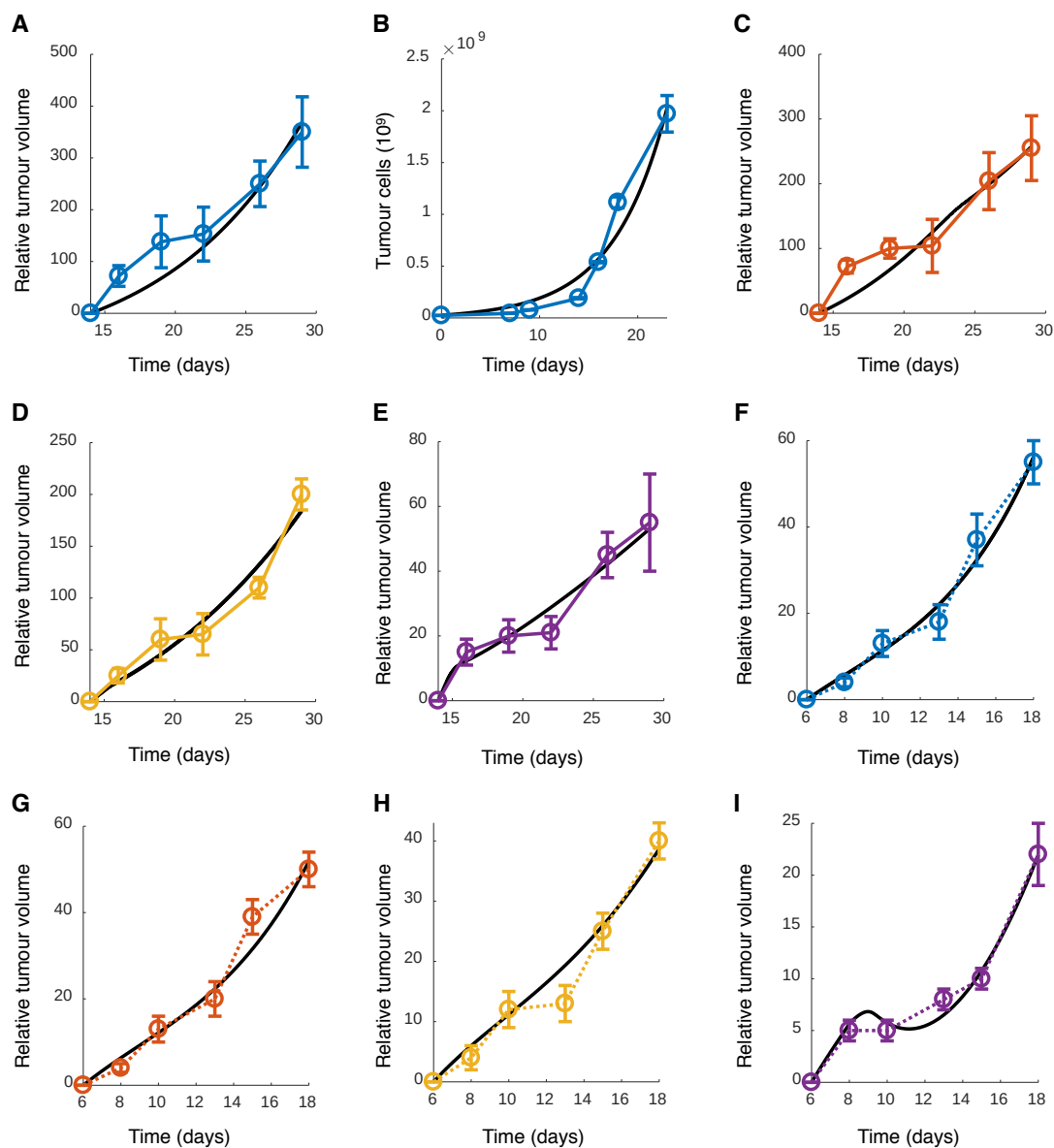
$$k_{cp} = \begin{cases} k_{cp} & t < N_E - 1 + D_B \\ k_{cp}^* & t \geq N_E - 1 + D_B \end{cases}$$

where N_E is the number of injections given daily (so $N_E - 1$ is the day the last enhancer is administered), and D_B is the lag (days) between the last VV injection and first VSV administration. We then estimated k_{cp}^*, ρ^* and δ_{VSV} by fitting the *4T1/IC-VV+VSV* data (see Fig. TS2I and Table TS2 & TS3).
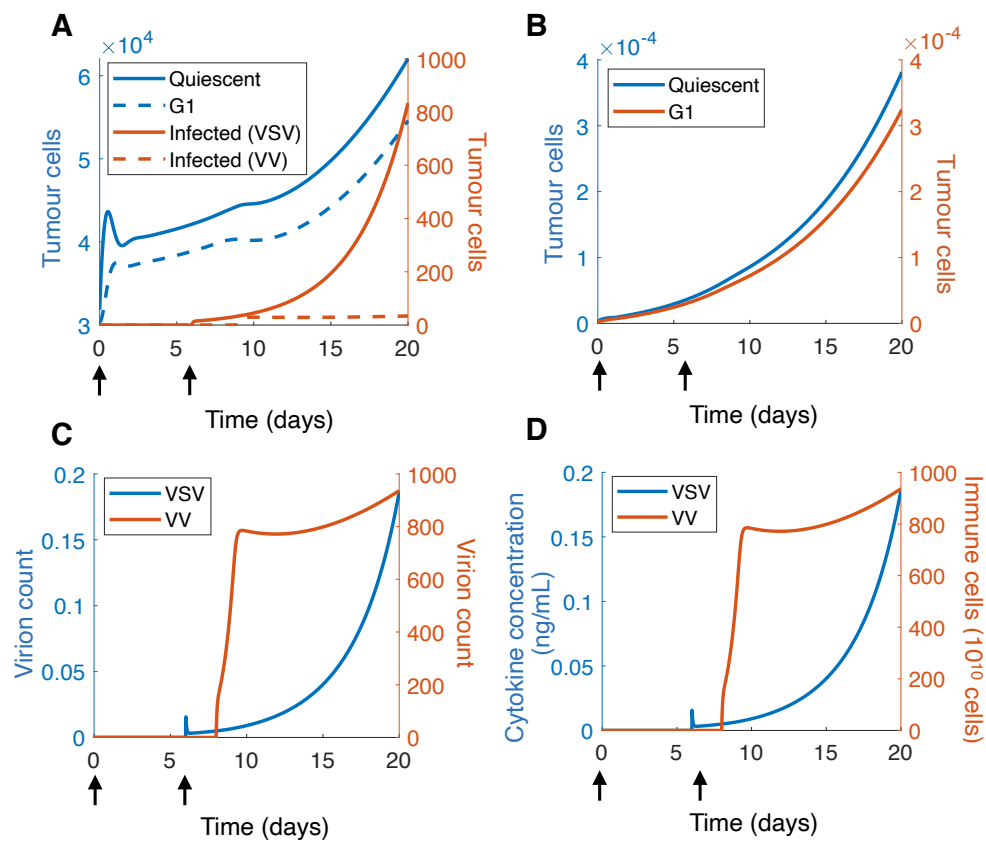
Overall, the model was able to produce qualitatively what was observed in the data with some minor exceptions. For the HT29 tumour model, initial growth measurements follow an extremely non-linear growth curve, which we were unable to capture exactly. The model dynamics exhibited in the *4T1/IC-VV+VSV* experiment are provided in Fig. TS3. From these estimates, we generated virtual individuals as described in the Main Text by parameterizing normal distributions around parameters so that 99.7% of patients fell within $[\mu - 3\sigma, \mu + 3\sigma] = [0.5\mathbf{p}, 1.5\mathbf{p}]$, where $\mathbf{p}$ is the vector of fitted parameters.

14

Param		HT29/ ID	4T1/ ID	HT29/ ID-VSV	HT29/ ID-VV	HT29/ ID-VV+VSV	4T1/ IC	4T1/ IC-VSV	4T1/ IC-VV	4T1/ IC-VV+VSV
a_1		**1.54**	**1.66**	1.54	1.54	1.54	1.66	1.66	1.66	1.66
a_2		**1.44**	**1.44**	1.44	1.44	1.44	1.44	1.44	1.44	1.44
d_2		**0.41**	**0.30**	0.41	0.41	0.41	0.30	0.30	0.30	0.30
κ_{VSV}				**0.066**		**0.066**	0.066			0.066
κ_{VV}					**0.054**	0.054			0.054	0.054
δ_{VSV}				**5.76**		**29.5**		**1.72**		**11**
δ_{VV}					**18.5**	18.5			**2.48**	2.48
α_{VSV}				**1.13**		**1.13**		1.13		1.13
α_{VV}					**1.12**	1.12			1.12	1.12
ω_{VSV}				*9.686*		*9.686*		**38.7**		38.7
ω_{VV}					*9.686*	*9.686*			**40.3**	40.3
k_p							**9.23**	9.23	9.23	9.23
$k_{q,s}$							**0.064**	0.064	0.064	0.064
$\Psi_{1/2}$							**1.1×10^{-4}**	1.1×10^{-4}	1.1×10^{-4}	1.1×10^{-4}
k_{cp}	t<8						*4.68*	4.68	4.68	*4.68*
	t>8									**3.08**
ρ	t<6						1	1	1	1
	6<t <8							0		0
	t>8							0		**0.995**

Table TS2. Estimated parameter values. *Parameters in bold are those that were fit to the data set noted by the column. Parameters in italics were values taken from Cassidy and Craig*[2]*. All other parameters were either estimated in a preceding fit and fixed for the resulting fits, or in the case of ρ were fixed to either 0 or 1 based on whether the immune response was upregulated or down regulated. Note that some parameters change with the introduction of the different viruses at t=6 and t=8 and this is labelled in the first column.*

Figure TS2. Parameter estimation results for VV and VSV in immunodeficient and immunocompetent mouse models. A) HT29/ID. B) 4T1/ID. C) HT29/ID-VV. D) HT29/ID-VSV. E) HT29/ID-VV+VSV. F) 4T1/IC. G) 4T1/IC-VV. H) 4T1/IC-VSV. I) 4T1/IC-VV+VSV. Data is represented by a coloured line joining circles for each data point. The colour of the line corresponds to whether the injection was control (blue), VV (orange), VSV (yellow) or VV+VSV (purple) for immunodeficient animals (solid data lines) or immune-competent animals (dotted data lines), with model predictions overlaid in black solid. Bars on each data point represent standard deviation.

16

Supplemental material

BMJ Publishing Group Limited (BMJ) disclaims all liability and responsibility arising from any reliance placed on this supplemental material which has been supplied by the author(s)

J Immunother Cancer

Figure TS3. Model dynamics for the 4T1/IC-VV+VSV model. *A) Number of cells in the Quiescent, G_1, VSV infected and VV infected populations as a function of time. B) Number of cells in the resistant quiescent and resistant G_1 populations as a function of time. C) Number of virions for the VSV and VV virus populations is plotted. D) Cytokine concentrations and immune cells as a function of time. The colour of the line determines its corresponding left (blue) or right (orange) y-axis. The time of the VV and VSV injections is noted by black arrows.*

17

Parameter	Units	Description	Value
a_1	1/day	Quiescent to interphase rate	1.66
a_2	1/day	Interphase to active phase rate	1.44
d_2	1/day	Interphase death rate	0.3
κ_{VSV}	1/day	VSV virion infection rate	0.066
κ_{VV}	1/day	VV virion infection rate	0.054
δ_{VSV}	1/day	VSV lysis rate	11
δ_{VV}	1/day	VV lysis rate	2.48
α_{VSV}	Virions/cell	VSV burst size	1.13
α_{VV}	Virions/cell	VV burst size	1.12
ω_{VSV}	1/day	VSV virion death rate	38.7
ω_{VV}	1/day	VV virion death rate	40.3
k_p	1/day	Phagocyte-tumour cell contact rate	9.23
$k_{q,s}$	-	Phagocyte cell digestion constant	0.064
$\Psi_{1/2}$	10^{10} cells/day	Cytokine production half effect	0.00011
k_{cp}	10^{10} cells/day	Maximal immune cell production rate	4.68 or 3.08
ρ	-	Immunomodulation constant	0 or 1

Table TS3. Mean parameter estimates used to generate the in silico individuals to investigate perturbations on the combination OV-therapy protocol using the 4T1/IC-VV+VSV model.
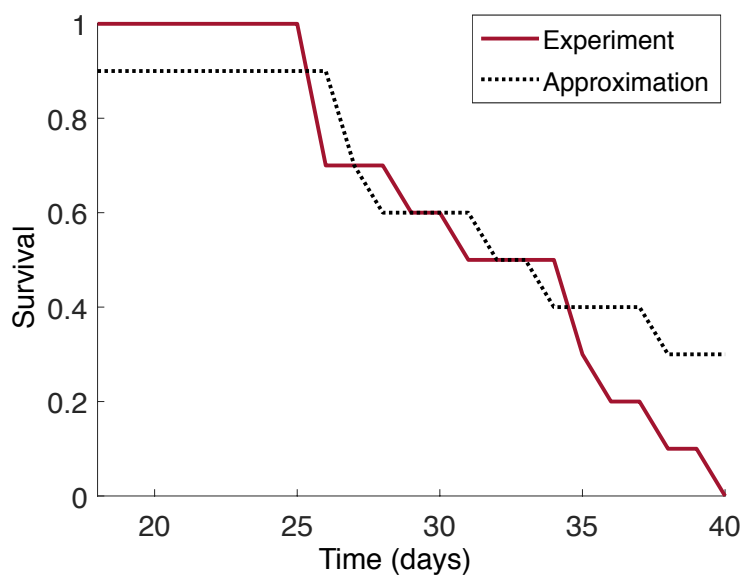
Parameter values were obtained from fitting the tumour growth measurements of Le Boeuf et al.[9] *and Rausch et al.*[12] *see Fig. TS3.*

18

Parameter	Units	Description	Value
d_1	1/day	Quiescent death rate	0
$\hat{d}_g$	1/day	Active phase death rate	0.167
$\eta_{1/2}$	Virions	Virion half effect concentration	0.51
$C_{1/2}$	ng/mL/day	Phagocyte production half effect	0.739
γ_p	1/day	Phagocyte death rate	0.35
C_{prod}^*	ng/mL/day	Homeostatic cytokine production rate	3.9210^{-4}
C_{prod}^{max}	ng/mL/day	Maximal cytokine production rate	1.429
k_{elim}	1/day	Cytokine elimination rate	0.16139
j	-	Number of transit compartments	9
k_{tr}	1/day	Transit rate	10.77
τ	-	Expected cell cycle duration	0.8354
μ	-	Proportion of resistant cells produced	10^{-10}
k_a^v	1/day	Virus absorption rate	20

Table TS4. Mean parameter estimates used to generate the in silico individuals to investigate perturbations on the combination OV-therapy protocol using the results from Cassidy and Craig[2]. *For a more detailed description of the parameters see Cassidy and Craig*[2] *or Cassidy and Humphries*[1].

Supplemental material

BMJ Publishing Group Limited (BMJ) disclaims all liability and responsibility arising from any reliance placed on this supplemental material which has been supplied by the author(s)

J Immunother Cancer

Determination of cumulative survival threshold

The cumulative survival Kaplan-Meier curves generated by Le Boeuf *et al.*[9] for their *4T1/IC-VV+VSV* model was used to determine a culling threshold for the mice cohorts in our virtual trial simulations. Le Boeuf *et al.* measured the proportion of mice with tumours below a certain threshold T^* alive from day 18 to day 40 after an injection of VV on day 6 and VSV on day 8 in 10 different mice (Fig. TS4). To recapitulate the observed survival, we randomly generated 50 cohorts with 10 different mice with mean tumour volume from the fitted curve for the *4T1/IC-VV+VSV* model in Table TS3 and Fig. TS2F. We then simulated tumour growth from day 18 to 40, and used a genetic algorithm to determine that value of T^* that lowered the residual between the cohorts we had generated, and the mice cohorts used by Le Boeuf *et al.* From this procedure, we found $T^* = 246,280$ cells.

Figure TS4. Comparison of cumulative survival thresholds*. Tumour size of mice at the culling threshold from results reported in Le Boeuf et al.[9] 4T1/IC-VV+VSV (maroon solid line) was approximated using our virtual trial and applied a genetic algorithm for 10 virtual mice (dotted line).*

Our algorithm would underestimate the tumour culling threshold if mice died prematurely to the threshold set by Le Boeuf *et al.*'s experiments, which could explain the discordance between our generated survival curves and the experimental data. Alternatively, the tumour aggressivity of the mice cohort could be varied differently to our virtual mice cohort, and this would result in a deviation of the cumulative survival curves. Either way, the survival curve approximation from our simulation shows

20

Supplemental material

BMJ Publishing Group Limited (BMJ) disclaims all liability and responsibility arising from any reliance placed on this supplemental material which has been supplied by the author(s)

J Immunother Cancer

qualitatively similar behavior and we use this culling threshold T^* in the calculation of the Kaplan Meier

survival curves.

REFERENCES

1 Cassidy T, Humphries AR. A mathematical model of viral oncology as an immuno-oncology instigator. *Math Med Biol* 2020;**37**:117–151. doi:https://doi.org/10.1093/imammb/dqz008

2 Cassidy T, Craig M. Determinants of combination GM-CSF immunotherapy and oncolytic virotherapy success identified through in silico treatment personalization. *PLoS Comput Biol* 2019;**15**. doi:10.1371/journal.pcbi.1007495

3 Cassidy T, Craig M, Humphries AR. Equivalences between age structured models and state dependent distributed delay differential equations. *Mathet Biosci Eng* 2019;**16**:5419–50.

4 Jenner A, Yun C-O, Yoon A, *et al.* Modelling heterogeneity in viral-tumour dynamics: The effects of gene-attenuation on viral characteristics. *J Theor Biol* 2018;**454**. doi:10.1016/j.jtbi.2018.05.030

5 Marshall HD, Urban SL, Welsh RM. Virus-induced transient immune suppression and the inhibition of T cell proliferation by type I interferon. *J Virol* 2011;**85**:5929–39.

6 Janeway Jr. CA, Travers P, Walport M, *et al. Immunobiology : the immune system in health and disease*. 6th ed. New York, NY: : Garland Science Publishing 2005.

7 Murray PR, Rosenthal KS, Pfaller MA. *Medical microbiology*. Elsevier Health Sciences 2015.

8 Lee S, Margolin K. Cytokines in cancer immunotherapy. *Cancers (Basel)* 2011;**3**:3856–93.

9 Le Boeuf F, Diallo JS, McCart JA, *et al.* Synergistic interaction between oncolytic viruses augments tumor killing. *Mol Ther* 2010;**18**:888–95. doi:10.1038/mt.2010.44

10 Telfer MG, Preston C, Rothery P. A general method for measuring relative change in range size from biological atlas data. *Biol Conserv* 2002;**107**:99–109.

11 Phelps VR. Relative index finger length as a sex-influenced trait in man. *Am J Hum Genet* 1952;**4**:1952.

12 Rausch MP, Hahn T, Ramanathapuram L, *et al.* An orally active small molecule TGF-β receptor I antagonist inhibits the growth of metastatic murine breast cancer. *Anticancer Res* 2009;**29**:2099–109.

13 Jenner ALAL, Yun COC-O, Kim PSPS, *et al.* Mathematical Modelling of the Interaction Between Cancer Cells and an Oncolytic Virus: Insights into the Effects of Treatment Protocols. *Bull Math Biol* 2018;**80**:1615–29. doi:10.1007/s11538-018-0424-4

14 Sadler AJ, Williams BRG. Interferon-inducible antiviral effectors. *Nat Rev Immunol* 2008;**8**:559–68.

15 Brown CM, Bidle KD. Attenuation of virus production at high multiplicities of infection in Aureococcus anophagefferens. *Virology* 2014;**466**:71–81.

16 Furness G, Youngner JS. One-step growth curves for vaccinia virus in cultures of monkey kidney cells. *Virology* 1959;**9**:386–95.

17 van den Pol AN, Davis JN. Highly attenuated recombinant vesicular stomatitis virus VSV-12′ GFP displays immunogenic and oncolytic activity. *J Virol* 2013;**87**:1019–34.

18 Le-Trilling VTK, Megger DA, Katschinski B, *et al.* Broad and potent antiviral activity of the

21

NAE inhibitor MLN4924. *Sci Rep* 2016;**6**:1–14. doi:10.1038/srep19977